AGU PUBLICATIONS

JGR

Journal of Geophysical Research: Earth Surface

RESEARCH ARTICLE
10.1002/2013JF002997

Key Points:
- Meandering with bank strength differences explains a variety of valley types
- The evolving distribution of alluvium and bedrock steers channel migration
- Alluvial rivers can entrench in bedrock without pulses of vertical incision

Supporting Information:
- Readme
- Movie S1
- Movie S2
- Movie S3
- Movie S4

Correspondence to:
A. B. S. Limaye,
ajay@caltech.edu

Citation:
Limaye, A. B. S., and M. P. Lamb (2014), Numerical simulations of bedrock valley evolution by meandering rivers with variable bank material, *J. Geophys. Res. Earth Surf.*, *119*, doi:10.1002/2013JF002997.

Received 30 SEP 2013
Accepted 3 APR 2014
Accepted article online 6 APR 2014

Numerical simulations of bedrock valley evolution by meandering rivers with variable bank material

Ajay B. S. Limaye[1] and Michael P. Lamb[1]

[1]Division of Geological and Planetary Sciences, California Institute of Technology, Pasadena, California, USA

Abstract Bedrock river valleys are fundamental components of many landscapes, and their morphologies—from slot canyons with incised meanders to wide valleys with strath terraces—may record environmental history. Several formation mechanisms for particular valley types have been proposed that involve changes in climatic and tectonic forcing, but the uniqueness of valley evolution pathways and the long-term stability of valley morphology under constant forcing are unknown and are not predicted in existing numerical models for vertically incising rivers. Because rivers often migrate more rapidly through alluvium than through bedrock, we explore the hypothesis that the distribution of bank materials strongly influences river meandering kinematics and can explain the diversity of bedrock river valley morphology. Simulations using a numerical model of river meandering with vector-based bank-material tracking indicate that channel lateral erosion rate in sediment and bedrock, vertical erosion rate, and initial alluvial-belt width explain first-order differences in bedrock valley type; that bedrock-bound channels can evolve under steady forcing from alluvial states; and that weak bedrock and low vertical incision rates favor wide, shallow valleys, while resistant bedrock and high vertical incision rates favor narrow, deep valleys. During vertical incision, sustained planation of the valley floor is favored when bedrock boundaries restrict channel migration to a zone of thin sediment fill. The inherent unsteadiness of river meandering in space and time is enhanced by evolving spatial contrasts in bank strength between sediment and bedrock and can account for several valley features—including strath terraces and underfit valleys—commonly ascribed to external drivers.

1. Introduction

The morphology of bedrock-floored river valleys is diverse. For example, deep slot canyons host highly sinuous channels (Figure 1a); wider mountain valleys include floodplains and stepped strath terraces (Figure 1b); confining valleys with relatively small width variations contain rivers that bend sharply at the valley walls (Figure 1c); and wide, low-sloping valleys can resemble alluvial river valleys (Figure 1d). The origin of such different valley types is a longstanding question in Earth surface science, and valley topography is commonly used to reconstruct channel kinematics [*Shyu et al.*, 2006; *Cook et al.*, 2009; *Finnegan and Dietrich*, 2011; *Finnegan and Balco*, 2013] and to infer drivers of landscape evolution including climate [*Molnar et al.*, 1994; *Hancock and Anderson*, 2002; *Pan et al.*, 2003], tectonics [*Lavé and Avouac*, 2000], and sea level [*Merritts et al.*, 1994; *Blum and Tornqvist*, 2000]. Understanding channel-valley interactions is an important consideration for stream restoration [*Wohl et al.*, 2005], especially in mountainous environments. Beyond Earth, valleys and valley networks are the most widespread indicators of fluid flow on the surfaces of Mars [*Baker*, 2001] and Titan [*Burr et al.*, 2013] and thus represent rare constraints on past and present climate. Linking valley type to channel hydrology and geomorphology, however, remains a significant challenge.

Although bedrock river valleys are key to landscape evolution, the diversity of valley types has not been explained quantitatively. Pulses of channel vertical incision have been argued to generate specific valley types, including deep and sinuous canyons (e.g., Figure 1a) [*Davis*, 1893] and broader valleys with flights of strath terraces [e.g., *Gilbert*, 1877; *Hancock and Anderson*, 2002; *Pan et al.*, 2003; *Finnegan and Dietrich*, 2011]. Other studies suggest rock strength as an important control on valley width [*Harden*, 1990; *Montgomery*, 2004; *Shyu et al.*, 2006; *Barbour*, 2008; *Finnegan and Dietrich*, 2011].

Despite these important studies, there are several major unknowns in how different valley types evolve. First, it is unclear whether changes in vertical incision rate are necessary to form particular valley types, or whether similar valleys can form under steady vertical incision rates. More generally, it is unknown whether multiple

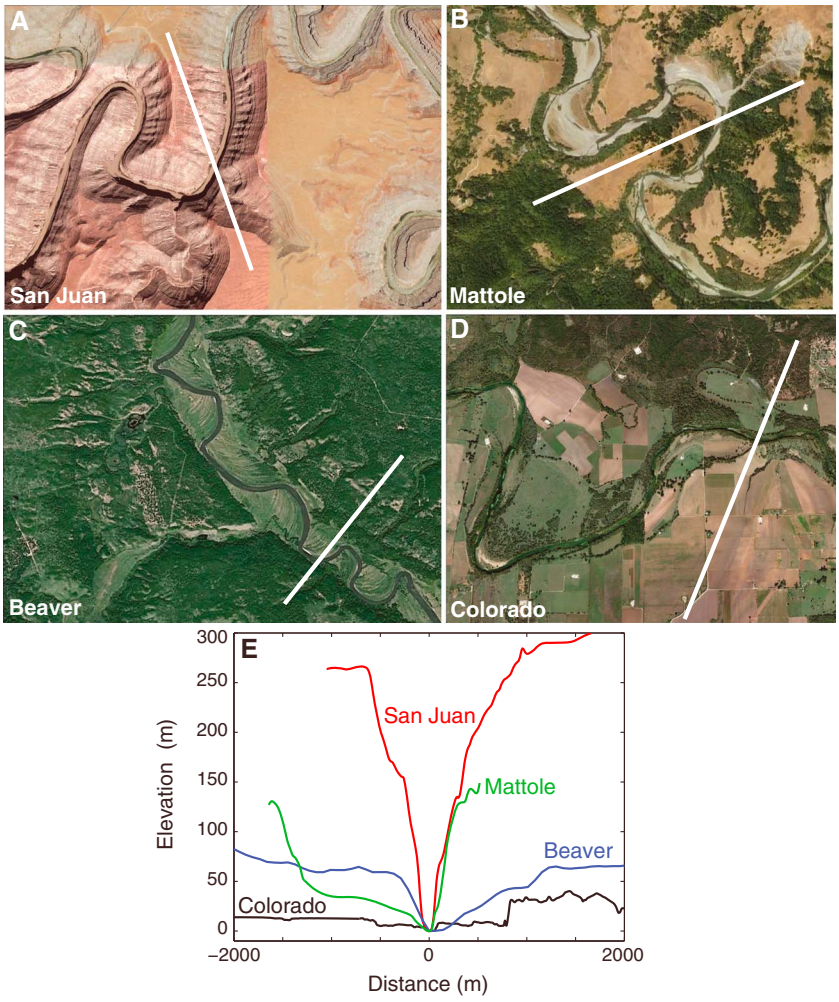

Figure 1. Bedrock river valleys with diverse morphologies. White lines denote topographic transects, all oriented from the lower portion of each image to the upper portion. (a) The San Juan River, Utah (37.2°N, 109.9°W). (b) The Mattole River, California (40.2°N, 124.2°W). (c) The Beaver River, Alberta, Canada (54.4°N, 110.4°W). (d) The Colorado River, Texas (30.2°N, 97.5°W). (e) Valley cross-section elevation profiles for valleys in Figures 1a–1d. Images: Google Earth/USDA Farm Service Agency/CNES Spot Image.

forcing mechanisms can lead to a particular bedrock valley type. Second, while previous work has suggested that vertical incision rate, lateral erosion rate, and bank strength may control valley topography, the relative importance of these independent variables has not been quantified. Third, it is unknown whether the different valley types observed in nature are stable, even under steady forcing, or whether they are transient. This distinction is vital for interpreting valley types for the history of river vertical incision—and by extension, the influences of tectonics, climate, and base-level on landscape evolution.

Bedrock river valleys evolve over millennial timescales, making it difficult to measure their dynamics directly [*Hancock and Anderson*, 2002; *Montgomery*, 2004]. Consequently, numerical experiments offer important means for testing controls on valley evolution. Numerous landscape evolution models have been used to explore river valley evolution and have reproduced valley features including strath terraces [*Hancock and Anderson*, 2002; *Finnegan and Dietrich*, 2011], meander bends that deform against valley walls [*Howard and Knutson*, 1984; *Howard*, 1992, 1996; *Sun et al.*, 1996], and meandering rivers with banks of different heights in uplifting mountain landscapes [*Lancaster*, 1998]. No model, however, reproduces the full diversity of bedrock river valley forms from incised meanders to wide valleys with terraces (Figure 1). Moreover, many larger-scale landscape evolution models represent valleys at scales too coarse to include valley evolution by lateral channel migration [*Howard et al.*, 1994; *Braun and Sambridge*, 1997].

Previous work on alluvial river floodplain development has shown that variable bank strength that evolves in response to channel migration can strongly control channel kinematics and meander-belt width [*Howard*, 1996; *Sun et al*., 1996]. Based on this insight, we hypothesize that bank strength that evolves dynamically in concert with river meandering is the key ingredient to explain the diversity of bedrock river valleys. For example, in narrow valleys with resistant bedrock walls (e.g., the San Juan River valley, Utah; Figure 1a), and wide valleys with weak bedrock walls (e.g., the Colorado River valley, Texas; Figure 1d), the consistency of channel bank materials results in meandering forms seemingly insensitive to valley geometry; rather, the bank materials control channel and valley evolution rates. In contrast, in intermediate-width valleys with large contrasts in bank strength between valley floor sediments and valley walls, channel migration is strongly influenced by bank strength, and meanders bend sharply at valley walls due to differential migration rates between the valley interior and margins (e.g., the Beaver River valley, Alberta, Canada; Figure 1c).

We aim to test the dynamic bank-strength hypothesis as follows. In section 2, we describe our specific modeling objectives and identify potential controls on valley evolution. In section 3, we describe the numerical framework used to model meandering channels and track bank-material properties. In section 4, we explore valley-type transitions under constant forcing. In section 5, we explore examples of valley-type transitions by pulses of vertical incision, which represents the kinematics of vertical incision driven, for example, by changes in sediment supply [e.g., *Hancock and Anderson*, 2002]. In section 6, we assess the ability of the numerical model to reproduce the observed bedrock river valley types and discuss implications for inferring valley evolution in section 7.

2. Modeling Goals and Hypotheses

Our modeling goal is to test the null hypothesis that the diversity of bedrock valley types can be explained without changes in external forcing that modulate channel vertical incision rate, but rather through the coevolution of channel lateral migration and bank strength under a constant vertical incision rate, as would correspond to a steady state longitudinal profile undergoing tectonic uplift [e.g., *Merritts et al*., 1994]. Although climate and tectonics likely force pulses in vertical incision rates in nature [e.g., *Molnar et al*., 1994; *Whipple and Tucker*, 1999; *Hancock and Anderson*, 2002; *Yanites et al*., 2010], it is important to understand the potential diversity of valley forms that can arise from intrinsic meandering dynamics as a baseline. Intrinsic dynamics may occur because as a channel migrates laterally, it can erode bedrock along the cutbank and channel bed and deposit sediment along the trailing bank, thus converting bedrock to sediment. Since channel migration rates are commonly faster in alluvium than in bedrock, this process should enhance lateral migration rates, relative to those in intact bedrock, in areas where the channel has previously visited. Bank materials are also affected by vertical incision rates because vertical incision lowers the channel bed with respect to the sediment-bedrock interface and thus favors bedrock exposure in the banks. Hence, we hypothesize that the competition of river lateral and vertical erosion determines the alluvial-belt width within a valley and the first-order valley topography.

In order to test this hypothesis, we construct the simplest possible model that can incorporate channel lateral migration and vertical incision, while tracking the spatial distribution of bedrock and sediment. In our model, the proportion of bedrock and sediment in the channel banks modulates channel lateral migration rates. We seek to balance the complexity inherent in river valley evolution—including meandering dynamics and evolving bank-material properties—with model simplicity in order to make predictions over 10^4 year timescales. We also seek to explain first-order differences in valley type in a generic way with as few controlling parameters as possible, which include time, bank strength, channel vertical incision rate, and the initial valley topography. A variety of other factors can influence channel geometry and evolution within valleys, including sediment supply [e.g., *Sklar and Dietrich*, 2001], channel slope [e.g., *Stark*, 2006; *Finnegan and Dietrich*, 2011], uplift rate [e.g., *Lavé and Avouac*, 2001; *Finnegan et al*., 2005; *Amos and Burbank*, 2007; *Yanites and Tucker*, 2010], discharge variability [e.g., *Turowski et al*., 2008; *Stark et al*., 2010], and channel substrate [e.g., *Ferguson*, 1973; *Finnegan et al*., 2005]. For example, a rapid decrease in channel width due to changes in uplift rate would transform the abandoned portions of the channel bed into strath terraces [*Lavé and Avouac*, 2001]. Here we exclude these diverse factors in order to isolate the how meandering with evolving bank strength alone influences valley evolution.

Table 1. Model Variables

Symbol	Description
	Dimensional Variables
w_c	Channel width
h_c	Channel depth
w_v	Valley width
h_v	Valley depth
w_{ab}	Initial alluvial belt-width
w_{uab}	Initial alluvial belt-width (unconfined)
C_f	Friction coefficient
E_V	Vertical incision rate
E_{Ls}	Lateral erosion rate in sediment
E_{Lb}	Lateral erosion rate in bedrock
k_e	Lateral erosion rate constant
k_s	Lateral erosion rate constant (sediment)
k_b	Lateral erosion rate constant (bedrock)
f_b	Fraction of bedrock in bank materials
Δt	Time step
t	Simulation time
Γ, Ω	Channel migration rate weighting coefficients
ξ	Distance along channel centerline
μ	Channel sinuosity
	Nondimensional Variables
$t^* = \frac{tE_{Ls}}{w_c}$	Nondimensional time
$E_{Vb}{}^* = \frac{E_V w_c}{E_{Lb} h_c}$	Nondimensional vertical incision rate with bedrock banks
$E_{Vs}{}^* = \frac{E_V w_c}{E_{Ls} h_c}$	Nondimensional vertical incision rate with sediment banks
$w_{ab}{}^* = \frac{w_{ab}}{w_{uab}}$	Nondimensional initial alluvial-belt width
$w_v{}^* = \frac{w_v - w_c}{h_v}$	Nondimensional valley width

A variety of channel meandering and bank evolution models exist, and their computational costs correspond to their complexity in representing factors including bed topography, hydraulics, and bank strength. Because significant computational costs are required for tracking bank-material properties over geologic timescales [*Limaye and Lamb*, 2013], we employ a relatively simple and often-utilized meandering model [*Howard and Knutson*, 1984] that imposes a fixed channel width and assumes erosion driven by channel curvature while still reproducing fundamental meandering kinematics [*Howard and Hemberger*, 1991]. Numerical models of river meandering are largely untested over geologic timescales [*Seminara*, 2006], but models with different degrees of complexity converge statistically for evolution beyond the stage of initial bend cutoff [*Camporeale et al*., 2005].

Although knickpoints can be important drivers of channel vertical incision [e.g., *Wobus et al*., 2006a; *Finnegan and Dietrich*, 2011], here we focus on constant and spatially uniform channel vertical incision, which will be shown to produce a wide range of valley types. The main difference between our work and most previous work is that we focus on the emergent, unsteady patterns of lateral migration for vertically incising rivers with evolving bank strength. Our approach is new because numerical experiments that account for differing channel migration rates within valleys and at their boundaries have been limited to cases with imposed geometries [*Tucker et al*., 2001], or without meandering [*Hancock and Anderson*, 2002] or channel vertical incision [*Howard and Knutson*, 1984; *Howard*, 1992, 1996; *Sun et al*., 1996]. Models that link meandering and vertical incision [*Lancaster*, 1998; *Finnegan and Dietrich*, 2011] have not incorporated evolving, mixed bedrock- and alluvial bank materials.

We define the channel as the zone of active sediment transport (of width w_c and depth h_c) that migrates laterally within a valley. We have identified seven characteristic parameters that we hypothesize control the geometry and kinematics common to mixed bedrock-alluvial, meandering channels, and their valleys, irrespective of the detailed mechanics of erosion and deposition. These are the lateral erosion rate in bedrock (E_{Lb}) and sediment (E_{Ls}), the vertical incision rate into a bedrock bed (E_v), channel width (w_c), initial alluvial-belt width (w_{ab}), channel depth (h_c), and the total simulation time (t) (Table 1). Using dimensional analysis, these seven parameters can be recast as five key dimensionless parameters: the dimensionless simulation time

$$t^* = \frac{tE_{Ls}}{w_c} \tag{1a}$$

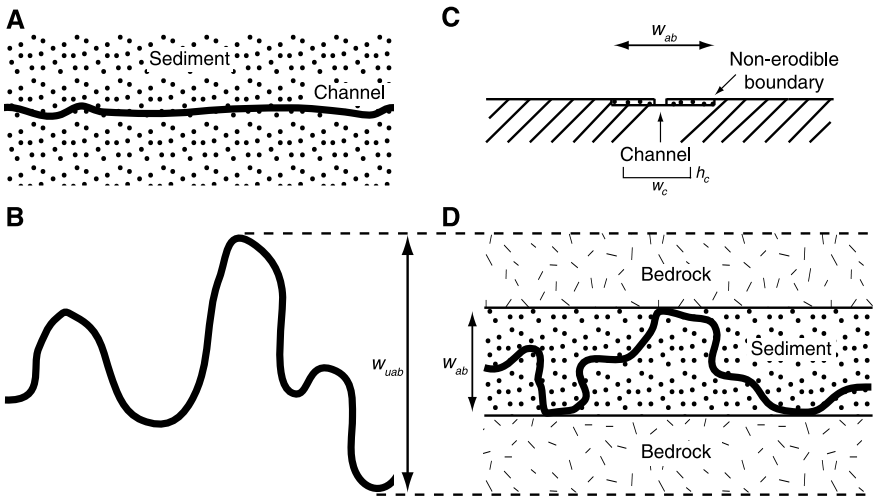

Figure 2. Model procedure for setting initial alluvial-belt width and channel planform geometry. The mean flow direction is from left to right. (a) A preliminary set of simulations is run to determine the maximum unconfined alluvial-belt width. The channel (black line) begins from a low-sinuosity state and has entirely sediment banks. (b) Each simulation is run until a fixed nondimensional time (t^*), at which the maximum range of the channel perpendicular to the mean flow direction is recorded as the unconfined alluvial-belt width (w_{uab}). (c) The channel is again evolved from a low-sinuosity state, but this time within a valley with impenetrable walls. The initial alluvial-belt width (w_{ab}) is a fraction $w_{ab}{}^*$ of the unconfined alluvial-belt width (w_{uab}). In this panel, $w_{ab}{}^* = 0.5$. This phase proceeds for a fixed nondimensional simulation time (t^*), and the channel may deform against the impenetrable walls. (d) For the start of the full simulation, the impenetrable valley walls are replaced with erodible bedrock walls. The banks are entirely sediment within the alluvial belt, and the depth of sediment is equal to the channel depth. Outside of the alluvial belt, and within the alluvial belt below the elevation of the channel bed, the landscape is entirely bedrock.

is the total simulation time normalized by the time to erode laterally one channel width in sediment; the dimensionless vertical incision rate with sediment banks

$$E_{Vs}{}^* = \frac{E_V w_c}{E_{Ls} h_c} \tag{1b}$$

is the characteristic time to erode one channel width in sediment normalized by the characteristic time to erode one channel depth; the corresponding dimensionless vertical incision rate with bedrock banks is

$$E_{Vb}{}^* = \frac{E_V w_c}{E_{Lb} h_c}. \tag{1c}$$

We select these two nondimensional vertical incision rate parameters to explore distinct regimes of channel migration in the simulations. $E_{Vs}{}^*$ reflects the competition between lateral channel mobility in sediment banks that actively bevels the bedrock-sediment interface, and vertical incision that drives the channel toward entrenchment in bedrock. In comparison, $E_{Vb}{}^*$ reflects the competition of lateral and vertical erosion in bedrock that should determine the evolution of valley topography if the channel has primarily bedrock banks. The channel width-to-depth ratio is

$$w_c{}^* = \frac{w_c}{h_c} \tag{1d}$$

and is fixed at 25 in our simulations. This value is representative of alluvial meandering channels for moderate valley slopes [e.g., *Parker*, 1976] and within the observed range for bedrock-alluvial rivers [*Yanites and Tucker*, 2010].

All simulations begin with a simple initial landscape condition: the channel is inset one depth in a level plane. All topography develops during the simulations as the channel simultaneously incises vertically and migrates laterally. The initial bank strength is locally set to represent either bedrock or sediment banks. To do this, we establish an initial zone of sediment fill one channel depth in thickness, such that the channel banks are composed entirely of sediment within this zone (Figure 2d), but the area's lateral margins and the channel bed are entirely bedrock. In cross section, the channel bed rests on a bedrock surface that extends across the valley and is mantled with sediment. Subsequent channel migration planes off the bedrock surface to the

channel bed elevation and emplaces sediment through point-bar accretion. To explore the influence of initial channel confinement on valley evolution, we vary the width of the initially sediment-mantled zone, which we call the initial alluvial-belt width (w_{ab}). We define a nondimensional initial alluvial-belt width (w_{ab}*)

$$w_{ab}* = \frac{w_{ab}}{w_{uab}} \tag{2}$$

where w_{uab} is a representative unconfined alluvial-belt width, defined as the maximum lateral distance (perpendicular to valley direction) between channel segments when the channel evolves without confinement by bedrock (Figure 2b). When $w_{ab}* = 0$, there is no initial alluvial belt, so the channel begins fully entrenched in bedrock. When $w_{ab}* = \infty$, the initial alluvial belt is infinitely wide and the channel banks are composed entirely of sediment. We explore these cases and cases with $0 < w_{ab}* < 1$, where there is a preestablished alluvial belt whose width is less than the unconfined width (Figure 2d).

We track the evolution of valley topography by calculating the valley aspect ratio

$$w_v* = \frac{w_v - w_c}{h_v} \tag{3}$$

where h_v is the median depth of the valley and w_v is the median valley width measured at the top of the valley. All areas lower than the elevation of the initial planar surface belong to the valley. In simulations that begin with low initial alluvial-belt confinement, the channel may initially sweep across a wide area before the influences of vertical incision rate and bedrock erodibility are expressed. In order to better characterize the typical valley width maintained during the simulation, we only consider topography that forms after the first channel depth of vertical incision (when the total incision exceeds one depth). Numerical experiments are designed to systematically vary the five controlling dimensionless parameters (equations (1a)–(1d) and (2)) and to track valley morphology and aspect ratio (equation (3)).

3. Model Formulation

In this section we describe methods for simulating meandering channel evolution, with bank strength feedbacks and vertical incision, over geologic timescales. We then detail procedures for setting the initial channel and alluvial-belt configurations.

3.1. Meandering Model Implementation

In the single-thread meandering channel model of *Howard and Knutson* [1984], the channel centerline migration rate responds to local and upstream-integrated curvature

$$R_1(s) = \Omega R_o(s) + \frac{\Gamma \int_0^{\xi_{max}} R_o(s-\xi)G(\xi)\mathrm{d}\xi}{\int_0^{\xi_{max}} G(\xi)\mathrm{d}\xi} \tag{4}$$

where R_1 is the dimensionless local migration rate, s is the centerline node index, ξ is the upstream distance, and $R_o = (r/w_c)^{-1}$, where r is the local centerline radius of curvature and w_c is channel width. Ω and Γ are fixed dimensionless parameters set to -1 and 2.5, respectively, and control the relative influence of local (Ω) and upstream (Γ) curvature [*Ikeda et al.*, 1981]. The numerator in equation (4) is a convolution integral of curvature with a weighting function

$$G(\xi) = e^{-\left(\frac{2kC_f}{h_c}\right)\xi} \tag{5}$$

where $k = 1$ [*Ikeda et al.*, 1981], h_c is the channel depth, and C_f is a dimensionless friction coefficient set to 0.01 after *Stølum* [1996]. Although channel hydraulics are not explicitly modeled, the friction coefficient reflects the downstream decay of velocity perturbations induced by local channel geometry. The dimensionless lateral migration rate is scaled according to the local lateral erosion rate constant (k_e, with dimensions LT^{-1}) and domain-averaged channel sinuosity (μ) to yield the dimensional lateral erosion rate

$$E_L = k_e R_1 \mu^{\varepsilon} \tag{6}$$

where $\varepsilon = -2/3$ [*Howard and Knutson*, 1984]. Therefore, lateral channel erosion rates, which are increased by high planform curvature of mature meander bends, are moderated as channel sinuosity increases.

The channel is assigned a rectangular cross section with fixed dimensions; the width and depth represent bankfull values. Consequently, the time step is fixed at 2 years to represent a typical recurrence interval of the bankfull discharge for an alluvial river [*Leopold and Wolman*, 1960]. While floods with longer the recurrence intervals may play a more important role in setting channel width in bedrock landscapes with large thresholds for sediment entrainment [*Baker*, 1977; *Hartshorn et al*., 2002; *Turowski et al*., 2008], there is considerable uncertainty in the appropriate adjustment timescale for bedrock rivers [*Tinkler and Wohl*, 1998] and the channel bed and banks may evolve on different timescales due to bed sediment cover effects [*Lague*, 2010]. In rivers with mixed bedrock and alluvial banks, the adjustment timescale may be closer to that for alluvial rivers; therefore, we fix the time step irrespective of the degree of channel entrenchment in bedrock.

We seek to vary the channel vertical incision rate as an independent parameter, which is commonly on the order of 0.1–1 mm/yr in tectonically active environments [*Montgomery*, 2004]. Slope breaks in meandering channel longitudinal profiles are a natural consequence, however, of bend growth and cutoff, and have been hypothesized to influence vertical incision rates [e.g., *Stark*, 2006; *Finnegan and Dietrich*, 2011]. To control the vertical incision rate for a sloping channel would then require static knickpoints [*Seidl and Dietrich*, 1992] that would increasingly dominate the channel longitudinal profile with each cutoff. Therefore, we set the channel slope to zero, which prevents knickpoint formation. Likewise, slope across the model domain is initially set to zero so that model landscape elevations can be measured with respect to the uniform channel elevation. The zero-slope assumption implies that model results for valley evolution should approach those for low-sloping rivers, except for modulation of vertical incision rates by slope reduction and knickpoint formation.

Neck cutoffs occur when the channel banks impinge upon themselves, and chute cutoffs are omitted in the model [e.g., *Sun et al*., 1996; *Lancaster*, 1998; *Finnegan and Dietrich*, 2011]. Overbank deposition is also omitted, except to fill in meander loops abandoned by cutoff [e.g., *Sun et al*., 1996; *Finnegan and Dietrich*, 2011], which is assumed to occur instantaneously. A periodic boundary condition is employed so that portions of the channel that drift outside the downstream edge of the model domain enter the upstream edge, and vice versa. Consequently, the channel axis is free to wander about the model domain and the curvature integration (equation (4)) is not affected by the domain boundaries.

3.2. Bank-Material Tracking

We track two classes of material: channel/floodplain sediments and bedrock. The local lateral erosion rate constant in equation (6) takes on distinct values in cases where the bank materials are entirely sediment ($k_e = k_s$) or entirely bedrock ($k_e = k_b$); these values represent the effects of sediment and bedrock strength on bank migration. Channel lateral migration rates for alluvial rivers often exceed several meters per year, with large variations between reaches [e.g., *Nanson and Hickin*, 1986; *Hudson and Kesel*, 2000]. For lateral migration in bedrock banks, rates rarely exceed a few cm/yr even for weak sedimentary rocks [*Montgomery*, 2004]. Although channel-widening processes in mixed bedrock-alluvial channels are a topic of active research [*Montgomery*, 2004; *Finnegan et al*., 2005; *Stark*, 2006; *Wobus et al*., 2006b; *Yanites and Tucker*, 2010], the influence of stratified sediment and bedrock on lateral erosion rates is relatively unconstrained [*Howard*, 1992]. In the simulations, we track the depth of sediment cover, and for simplicity, the local bank erodibility is scaled according to the local fraction of bedrock (f_b) in the bank material measured from the channel bed to the bankfull elevation

$$k_e = k_s(1 - f_b) + k_b f_b. \tag{7}$$

This fraction represents the amount of bedrock that would be exposed by the channel banks if the channel were to migrate to that portion of the landscape without further vertical incision. The bank-material bedrock fraction is useful for visualizing the width of the alluvial belt that is conducive to relatively rapid channel lateral migration.

Most existing approaches to modeling the coevolution of meandering channels, floodplains, and valleys use grids to represent factors that may influence bank migration rates, such as topography [*Lancaster*, 1998] and bank-material susceptibility to erosion [*Howard*, 1996; *Sun et al*., 1996]. Grid-based bank-material tracking, however, can implicitly impart thresholds for channel migration when bank strength varies spatially; this inadvertently suppresses lateral erosion as a result of numerical artifacts [*Limaye and Lamb*, 2013]. Consequently, we employ a new, vector-based method for bank-material tracking that more faithfully captures the kinematics of channel migration driven by an underlying meandering model without the

resolution effects of grid-based approaches [*Limaye and Lamb*, 2013]. This method uses the time history of channel planform and longitudinal profile geometry to reconstruct bank-material properties and topography in areas influenced by channel migration and thus avoids losses in geometric information commonly incurred from mapping the channel banks onto a relatively coarse grid. The vector-based method is particularly advantageous in scenarios with large differences in bank strength, as is commonly the case when comparing bedrock and sediment bank materials.

Depending on the process of bank erosion, increasing bank height could inhibit lateral migration by requiring removal and transport of more sediment [*Hickin and Nanson*, 1975; *Lancaster*, 1998; *Seminara*, 2006; *Parker et al*., 2011], which can be incorporated into our model framework [*Limaye and Lamb*, 2013]. However, here we make the lateral erosion rate independent of bank height to focus on the effect of bank strength.

3.3. Initialization of Alluvial-Belt Width and Channel Planform Geometry

We wish to explore a range of initial alluvial-belt widths, from $w_{ab}^* = 0$ to ∞, to which the channel is initially confined. As a result, the same sinuous channel centerline cannot be used to begin all simulations because in some cases, the channel would extend beyond the initial alluvial belt. Therefore, we develop an initialization procedure that produces a channel that is sinuous but confined to an initial alluvial belt of arbitrary width. As a preliminary step, we empirically determined a representative unconfined alluvial-belt width from a set of 50 simulations. In each, the channel had sediment banks and grew from an initially straight channel centerline seeded with meter-scale random noise (Figure 2a) for a fixed nondimensional simulation time ($t^* = 500$, equivalent to $t = 25$ kyr for $w_c = 50$ m and $E_L = 2$ m/yr, for example) to allow the channel to mature through several cycles of meander bend growth and cutoff. The mean unconfined alluvial-belt width ($w_{uab} = 2538$ m), measured perpendicular to the mean flow direction (Figure 2b), was used in subsequent simulations.

The model initialization phase establishes a realistic geometry for the channel where it meets confining bedrock walls by first evolving the channel within the alluvial belt bounded by nonerodible walls, and without vertical incision (Figure 2c). When $0 < w_{ab}^* < \infty$, the meander bends can deform against the nonerodible walls but do not advance beyond them. At the end of the initialization phase ($t^* = 500$), the channel planform geometry is recorded and used to begin the main simulation. The model time starts at $t^* = 0$, and the nonerodible walls are replaced with erodible bedrock walls (Figure 2d).

Meandering channel planform evolution is highly sensitive to initial geometry [e.g., *Frascati and Lanzoni*, 2010], and we have found this behavior is reinforced by strong feedbacks between meandering and bank strength. The channel trajectory in turn determines the pattern of erosion within the valley. Therefore, we assess the sensitivity of final valley aspect ratio to initial conditions by running the simulations for each unique set of parameter values in triplicate, each time with a different initial, sinuous planform geometry reflecting different noise in the channel centerline used during the simulation initialization phase.

4. Controls on Bedrock Valley Type Under Constant Forcing

We begin this section by exploring independently the influence of nondimensional simulation time (t^*), initial alluvial-belt width (w_{ab}^*), and vertical erosion rate with sediment banks (E_{Ls}^*) and bedrock banks (E_{Vb}^*), on the evolution of meandering rivers in bedrock valleys. The channel dimensions are fixed at $w_c = 50$ m and $h_c = 2$ m. In section 4.5, we introduce a method for objectively classifying valley type and summarize results for a suite of simulations that span a wide parameter space in the nondimensional variables.

4.1. Temporal Evolution

In this section, we analyze the evolution of a meandering river and its bedrock valley for a baseline simulation to which we will compare results from other simulations. The chosen parameters fall in the midrange of parameters explored in this study ($E_{Vb}^* = 0.5$; $E_{Vs}^* = 0.005$, $w_{ab}^* = 0.5$), which correspond to a river with moderate bedrock erodibility, vertical incision rate, and initial alluvial-belt confinement. In subsequent sections, we perturb this base case by fixing the nondimensional simulation time ($t^* = tE_{Ls}/w_c$; equation (1a)) and varying one of the other nondimensional parameters in order to isolate its influence on model results. Figure 3 shows the shaded relief of the land surface for the base case at different times, where the coloration indicates the local fraction of bedrock versus alluvium in the bank materials. We vary t^* from 0 to 1000 (Movie

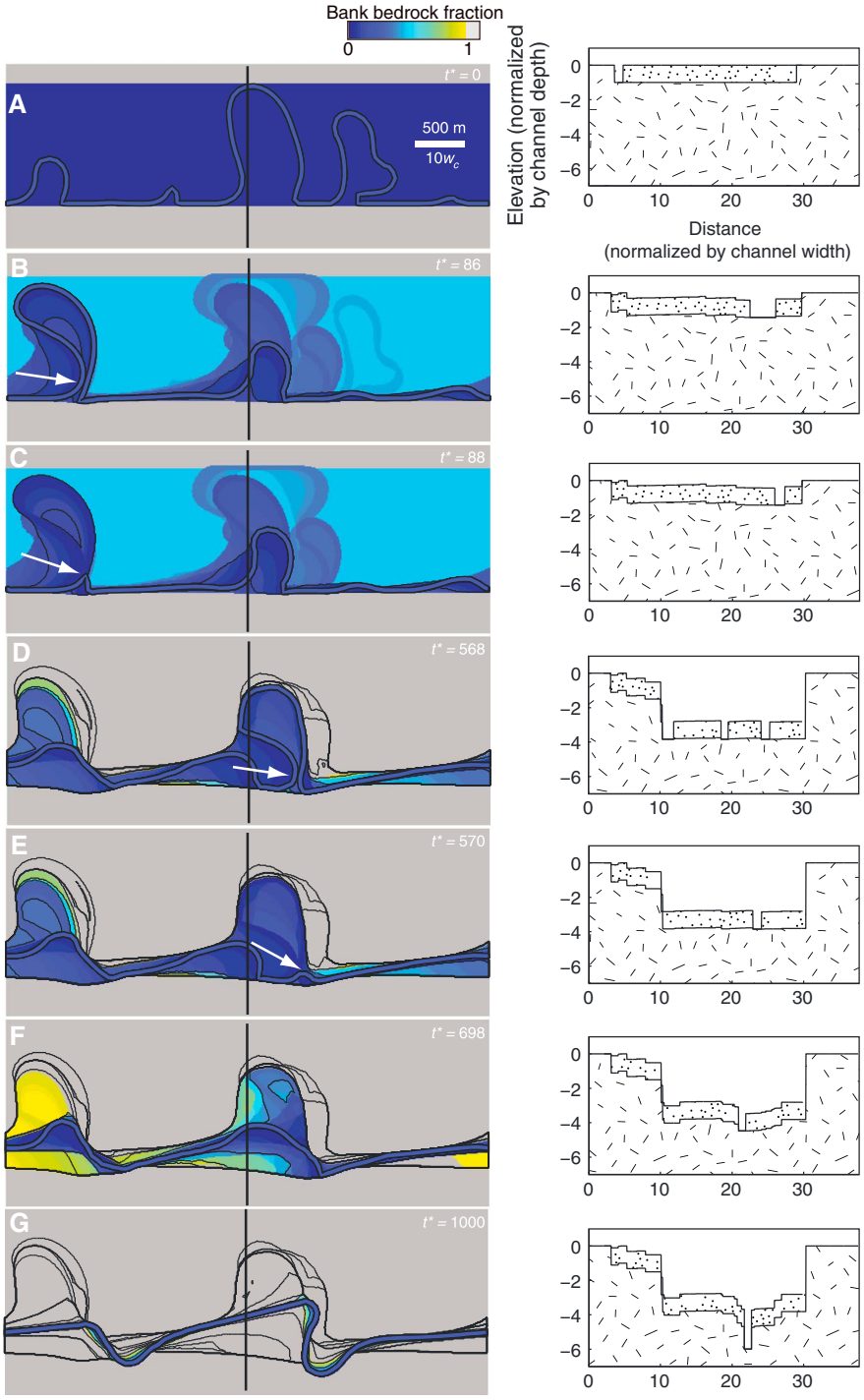

Figure 3. Snapshots of channel and valley evolution under constant vertical incision. The left side of each panel shows the shaded relief topography, with a fixed contour interval of 0.5 channel depths (equal to 1 m here and in all simulations). The mean flow direction is from left to right. The width of the model domain is 100 channel widths, and the scale is consistent for all map-view panels. The coloration represents the fraction of bedrock (f_b) in bank materials that the channel would encounter if it migrated laterally into that portion of the landscape with no change in its vertical position. For areas in gray $f_b = 1$, indicating that if the channel were to migrate to those areas, it would encounter entirely bedrock in the bank up to the bankfull depth. Also shown are the channel planform extent (blue), top-to-bottom topographic profile locations (black), and the nondimensional simulation time (t^*). The right side of the figure shows valley cross sections, including bedrock (hatched areas) and sediment (stippled areas). Model parameters are $t^*_{max} = 1000$, $E_{Vs}^* = 0.005$, $E_{Vb}^* = 0.5$, and $w_{ab}^* = 0.5$, which represent the base case parameters. Where white arrows appear, they indicate the locations of neck cutoffs. (a–g) Valley and channel state at times from $t^* = 0$ to 1000. The end state in Figure 3g is also shown in Figure 5b.

S1 in the supporting information), which corresponds to timescales up to tens of kiloyears for alluvial rivers with widths of 10–100 m.

At the beginning of the simulation ($t^* = 0$; Figure 3a), the river is sinuous and laterally mobile, and bends at sharp angles where it meets bedrock walls. Sediment with thickness equal to the channel depth is distributed across the uniform-width alluvial belt. As time advances, this simulation shows major reductions in short-wavelength ($\leq 15\ w_c$) channel sinuosity and average alluvial-belt width. We observe the following sequence involving the interplay of lateral channel migration and vertical incision, which leads to channel autogenic entrenchment in bedrock. Channel bends tend to sweep in the downstream direction, as is commonly observed in nature in the absence of bank strength differences [*Howard*, 1992]. Despite its initial mobility, the channel sweeps laterally across the valley in an uneven manner because of the spatial variability in local channel curvature and lateral erosion rates. With ongoing vertical incision, this unsteady channel lateral migration results in spatial variations in the fraction of bedrock in bank materials (Figure 3b). The downstream limb of a meander bend tends to plane off the bedrock-sediment interface in advance of the arrival of the upstream limb, so that the cutbank of the upstream limb commonly encounters bank materials with low bedrock fractions. Conversely, the cutbank on the downstream limb encounters areas with heterogeneous bank strength due to irregular channel sweeping (Figure 3b), though no bank materials within the initial alluvial belt are all bedrock (i.e., $f_b < 1$). Because the upstream bend limb encounters uniformly weak bank materials along the cutbank, but the downstream limb encounters bank materials with a range of strengths along the cutbank, the downstream limb eventually propagates more slowly than the upstream limb. The upstream limb catches up with the downstream limb, causing a neck cutoff (Figure 3c). Thus, the frequency and locations of cutoffs evolve with the changing fraction of bedrock in bank material.

This cutoff mechanism does not occur at the same time for all bends, and so the channel is straighter in some reaches than others. As the channel continues to incise, bends encounter local bedrock constrictions (i.e., $f_b = 1$) (Figure 3d). These constrictions strongly inhibit the downstream movement of downstream bend limbs, resulting in more cutoffs (Figure 3e). Eventually, cutoffs remove so much low-wavelength sinuosity ($\leq 15\ w_c$) that the diminished curvature causes channel lateral migration to stall, even while the banks are largely sediment in some locations (Figure 3f). In the absence of continued channel lateral migration, the sediment-bedrock interface is no longer lowered across a broad alluvial belt, so continued vertical incision causes the low-sinuosity channel to become more entrenched locally in bedrock (Figure 3g). These results suggest a pathway for channel entrenchment that can occur without a pulse of vertical incision—but that instead emerges through the interplay of channel meandering and vertical incision in a mixed bedrock-alluvial valley.

This baseline simulation also indicates that the valley type observed for a set of model parameters depends on the time of observation. Valley types that are seemingly stable, such as those with partially confined alluvial belts (Figures 3a–3c), can abruptly change in planform morphology due to the interaction of irregular lateral migration with vertical incision, resulting in a change in channel entrenchment state (Figure 3g). Given this inherent instability in valley type, in subsequent model comparisons, we fix the time of observation to $t^* = 1000$. This is sufficient time for the fastest-migrating bends to migrate laterally against sediment banks a total distance of approximately 1000 channel widths. For $w_c = 50$ m and $E_{Ls} = 2$ m/yr, for example, this is equivalent to $t = 25$ kyr.

4.2. Nondimensional Initial Alluvial-Belt Width (w_{ab}*)

In this section we isolate the influence of nondimensional initial alluvial-belt width ($w_{ab}{}^* = w_{ab}/w_{uab}$; equation (2)) on valley type by exploring the full range of possible initial alluvial-belt widths while holding other model parameters fixed at the values for the baseline case ($t^* = 1000$; $E_{Vb}{}^* = 0.5$; $E_{Vs}{}^* = 0.005$). As defined in Figure 2, the alluvial belt is a region of uniform-width sediment fill, with thickness equal to the channel depth, and represents the zone in which the channel can initially migrate against entirely sediment banks. Figure 4 shows simulation results for initial alluvial-belt widths of $w_{ab}{}^* = 0$ (a bedrock plain with a channel inset by one depth), 0.75 (a region of alluvium one channel deep, with a finite width), and ∞ (a broad blanket of alluvium one channel deep across the entire domain).

For $w_{ab}{}^* = 0$ (Figure 4a), the sinuous channel is initially surrounded by fully bedrock banks. As a result, meander bends largely migrate into bedrock for the entire simulation, leaving sediment-mantled slip-off surfaces behind them. In the time allowed, three bends migrate to the point of reaching cutoff. The valley

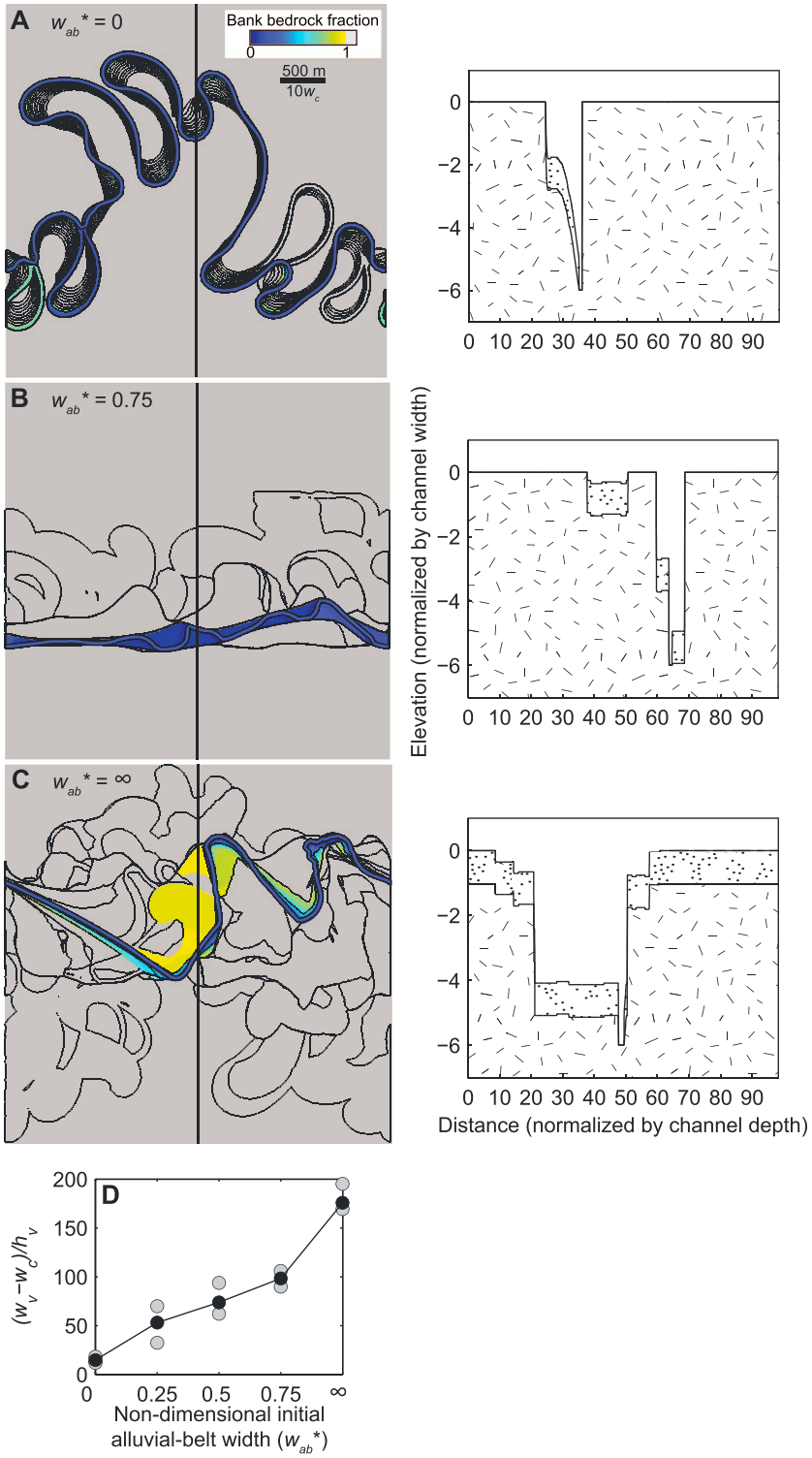

Figure 4. Valley topography formed for different initial alluvial-belt widths, where w_{ab}* represents the ratio of the initial alluvial-belt width to the unconfined alluvial-belt width. Symbols and coloration are the same as in Figure 3; the scale is identical in all map-view panels and the mean flow direction is from left to right. All simulations use the base case parameters other than w_{ab}* (t* = 1000, E_{Vs}* = 0.005, and E_{Vb}* = 0.5). Map views are shown for (a) a valley with no initial alluvial belt (w_{ab}* = 0), (b) a valley with a partially confined initial alluvial belt (w_{ab}* = 0.75), and (c) a valley with a fully unconfined initial alluvial belt (w_{ab}* = ∞). (d) Valley aspect ratio versus w_{ab}* for five simulations run in triplicate with different initial channel planform geometries. The median valley aspect ratio for each value of w_{ab}* is shown in black.

cross section shows that much of the valley remains entirely bedrock, similar to the valley cross-section topography of the San Juan River (Figure 1a), for example, except for a greater prevalence of slip-off surfaces and cutoff loops in the model case.

For $w_{ab}^* = 0.75$, the sinuous channel is initially partially confined and deforms against the valley walls. As the system evolves, channel migration becomes confined to an ever-narrower portion of the valley (Figure 4b; Movie S2 in the supporting information) because the channel does not sweep laterally frequently enough to bevel the bedrock-sediment interface to the level of the incising channel bed. Consequently, the channel encounters a significant fraction of bedrock in the banks except in areas recently visited by the channel. The alluvial-belt width at $t^* = 1000$ varies across the model domain (Figure 4b). Within the valley, the channel is sinuous in places but deforms strongly against areas with all-bedrock banks. If the channel were to frequently sweep across the entire alluvial belt, it would bevel the valley floor to a consistent elevation and would not leave any terraces, but incomplete sweeping of the alluvial belt during vertical incision causes the abandonment of sediment-mantled bedrock surfaces as strath terraces. After five depths of vertical incision, the channel occupies a narrow valley floor ($< 10\ w_c$) filled with alluvium.

For $w_{ab}^* = \infty$ (Figure 4c; Movie S3 in the supporting information), the full model domain is mantled with sediment to one channel depth. The channel initially wanders across a large area, but lateral migration slows dramatically because the channel does not sweep across the same portion of the model domain frequently enough to plane off the bedrock-sediment interface across the broad initial alluvial belt. Areas of low bank bedrock fraction are largely restricted to slip-off surfaces, and like the case with $w_{ab}^* = 0.75$ (Figure 4b), there are widespread terraces. The channel planform retains sinuosity at long wavelengths ($> 15\ w_c$) but has low sinuosity at shorter wavelengths, which reduces lateral erosion rates. The valley cross section shows the extent of the initial sediment cover preserved at the edges of the model domain, but interestingly, the channel ends the simulation largely bound in bedrock, similar to the case with $w_{ab}^* = 0$. As a more straightforward consequence of initial alluvial-belt dimensions, the valley aspect ratio shows that wider valleys form when w_{ab}^* is larger (Figure 4d) because the initial sediment banks enable widespread channel migration (Figure 4c).

The most surprising result from comparing simulations that vary the initial alluvial-belt width is that channels that begin with partially confined alluvial belts ($w_{ab}^* = 0.75$; Figure 4b) are able to maintain mobility in sediment banks more than channels that begin with either no alluvial belt ($w_{ab}^* = 0$; Figure 4a) or one of infinite width ($w_{ab}^* = \infty$; Figure 4c). A partially confined alluvial belt steers the channel to frequently plane off the bedrock-sediment interface over a narrow zone, which ensures that the bank materials there are largely sediment. The alluvial-belt boundaries are eroded into arcs with wavelengths that are longer than that of a free meander bend (Figure 4b), reflecting bend deformation and translation parallel to the boundaries. If there is no initial alluvial belt, the bank-material properties initially exert no control on the spatial pattern of erosion, only the rate of planform evolution. Consequently, the channel laterally migrates over significant distances before it reoccupies an area where it has planed off the bedrock and emplaced sediment. The bank bedrock fraction therefore remains high throughout the simulation. On the other hand, a channel that begins with an infinite-width alluvial belt can initially migrate freely over a wide swath of the model domain, with no steering of channel migration by alluvial-belt boundaries. The channel cannot plane off this entire area frequently enough to stave off an increase in entrenchment due to ongoing vertical incision, and the channel eventually reaches a less mobile, bedrock-bound state resembling that in the $w_{ab}^* = 0$ case.

In subsequent sections, we fix the nondimensional initial alluvial-belt width to an intermediate value ($w_{ab}^* = 0.5$), which produces a partially confined state. Simulations with partially confined initial alluvial belts generally allow greater variety in valley state after $t^* = 1000$ than simulations with either nonexistent or infinitely wide initial alluvial belts.

4.3. Nondimensional Vertical Incision Rate With Sediment Banks (E_{Vs}^*)

In the next set of simulations, we vary the nondimensional vertical incision rate with sediment banks ($E_{Vs}^* = (E_V w_c)/(E_{Ls} h_c)$; equation (1b)) while fixing other model parameters to their baseline values ($t^* = 1000$; $E_{Vb}^* = 0.5$; $w_{ab}^* = 0.5$). The initial channel and alluvial belt geometries are similar to those at $t^* = 0$ for the baseline case (Figure 3a). We vary E_{Vs}^* from 0.001 to 0.01, reflecting a range in dimensional vertical incision rates from a low of 0.08 mm/yr (i.e., a slowly uplifting continental interior environment) to

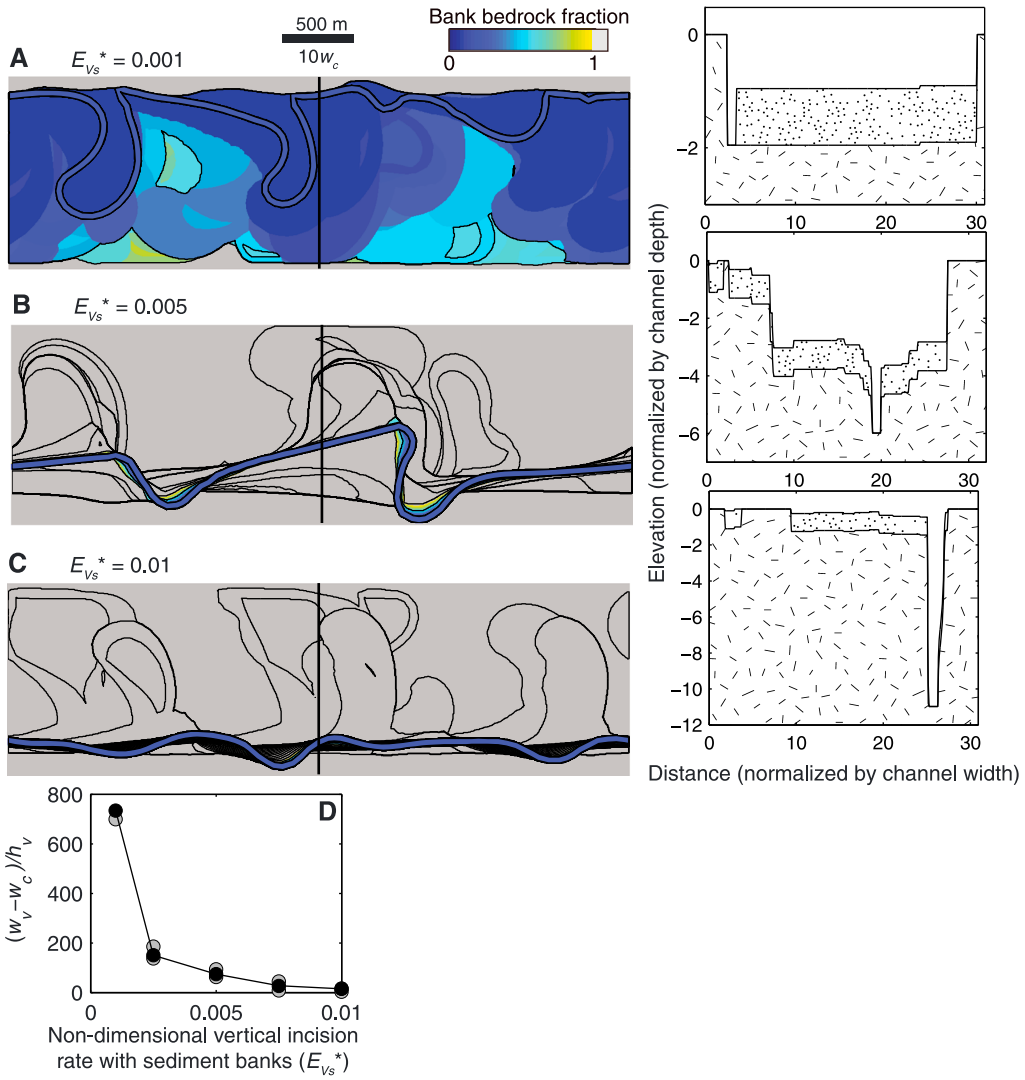

Figure 5. Topography of valleys formed by initially high-sinuosity channels for different values of nondimensional vertical incision rate with sediment banks (E_{Vs}*). All simulations use the base case parameters other than E_{Vs}* (w_{ab}* = 0.5, t* = 1000, and E_{Vb}* = 0.5). Symbols and coloration are the same as in Figure 3; the scale is identical in all map-view panels and the mean flow direction is from left to right. Map views are shown for (a) E_{Vs}* = 0.001, (b) E_{Vs}* = 0.005, and (c) E_{Vs}* = 0.01. (d) Valley aspect ratio versus E_{Vs}* for five simulations run in triplicate with different initial channel planform geometries. The median valley aspect ratio for each value of E_{Vs}* is shown in black. Figure 5b corresponds to the final time of the baseline case (Figure 3g).

a high of 0.8 mm/yr (i.e., an active orogen) for our scaled river example (i.e., w_c = 50 m, h_c = 2 m). E_{Vs}* should control the tendency of the channel to plane laterally and maintain an alluvial belt versus incise vertically and entrench in bedrock, and so is relevant when channels encounter a large fraction of sediment in the banks. E_{Vb}* is explored in the next section and should dictate valley topography for largely bedrock-bound channels.

Figures 5a–5c show map views of topography and local bank-material bedrock fraction for increasing values of E_{Vs}*. Overall, as E_{Vs}* increases, channel sinuosity, alluvial-belt width, and valley width decline, and meander bends more commonly encounter valley walls. For a relatively small value of E_{Vs}* (0.001; Figure 5a; Movie S4 in the supporting information), the channel is able to maintain a consistently wide alluvial belt compared to the baseline case (Figure 3g) because the channel incises minimally during lateral migration and a low bank bedrock fraction is maintained across the valley. Meander bends curve smoothly in sediment-filled areas but turn sharply where the channel meets resistant bedrock walls near the top edge of the model domain. The valley cross section shows only slight variation in the depth to bedrock. For a moderate value of

E_{Vs}* (0.005; Figure 5b), meander bend amplitude at short wavelengths (≤ 15 w_c) is reduced, and the valley width indicated by the topographic contours varies considerably. The valley cross section shows that the total depth of incision is larger than in Figure 5a because of the higher vertical incision rate. For a large value of E_{Vs}* (0.01; Figure 5c), the amplitude of long-wavelength bends (> 15 w_c) is also reduced. The valley cross section shows a stranded surface from the initial alluvial belt, and the deeply bedrock-bound channel. The valley aspect ratio (Figure 5d) declines sharply as E_{Vs}* increases because of increased channel entrenchment in bedrock, which limits valley widening during vertical incision.

4.4. Nondimensional Vertical Incision Rate With Bedrock Banks (E_{Vb}*)

Figure 6 shows results of simulations in which vertical incision rate with bedrock banks ($E_{Vb}^* = (E_{Vb}w_c)/(E_{Ls}h_c)$; equation (1c)) is varied while fixing other parameters to their baseline values ($t^* = 1000$; $E_{Vs}^* = 0.005$; $w_{ab}^* = 0.5$). The initial channel and alluvial-belt geometry is similar to that at $t^* = 0$ for the baseline case (Figure 3a). We vary E_{Vb}* from 0.05 to 5 by using a range of dimensional bedrock lateral erosion rates from 2 mm/yr (i.e., highly resistant lithologies) to 20 cm/yr (poorly consolidated valley fill sediments).

For $E_{Vb}^* = 0.05$ (Figure 6a), a broad valley forms and the channel maintains its short-wavelength sinuosity (≤ 15 w_c) because the channel can substantially erode bedrock valley walls even in a bedrock-entrenched state. The topographic cross section highlights the breadth of the alluviated zone and unpaired terraces of different widths. For $E_{Vb}^* = 5$ (Figure 6b), the alluvial-belt width varies substantially. As was the case for previous simulations, local suppression of channel migration by bedrock banks led to further reduction in channel sinuosity and increased entrenchment in bedrock. The valley aspect ratio (Figure 6c) declines as E_{Vb}* increases because higher E_{Vb}* favors channel vertical incision over lateral channel migration in bedrock. More scatter exists in the valley aspect ratio than for w_{ab}* (Figure 4d) and E_{Vs}* (Figure 5d) because in the present simulations, the valley widened during both the transient period in the beginning of the simulation when the channel had alluvial banks (as occurred in previous cases, including Figure 3a–3c) and during the bedrock-entrenched phase when the bedrock was relatively weak (Figure 6a). Thus, E_{Vb}* explains the most variance in valley aspect ratio when the channel consistently has largely bedrock banks.

The bank strength contrast, which we define as the ratio of bedrock lateral erosion rate to sediment lateral erosion rate (equivalent to k_s/k_b in equation (7)), covaries with both the dimensionless vertical incision rate with sediment banks (E_{Vs}*) and the corresponding rate with bedrock banks (E_{Vb}*). The primary effect of the bank strength contrast is that for a valley with an alluvial belt of significant width, low bank strength contrast causes smoothly curved meander bends (Figure 6a, $k_s/k_b = 10$), whereas high bank strength contrast causes meander bends to deform strongly at the margins of the alluvial belt (Figure 5b, $k_s/k_b = 100$).

4.5. Summary of Model Predictions for Valley Type

Here we analyze simulations that span a phase space in the variables t^*, w_{ab}*, E_{Vs}*, and E_{Vb}*, in order to systematically assess controls on bedrock river valley type. In all cases, the parameters that are not systematically varied are set to values employed in the baseline simulation.

The morphology of bedrock river valleys spans the examples shown in Figure 1. These include deep, narrow canyons (e.g., San Juan River valley; Figure 1a) and valleys with local floodplain and strath terrace development and channel confinement (e.g., Mattole River valley; Figure 1b); valleys with relatively uniform floodplain widths and pronounced bend deformation against valley walls (e.g., Beaver River valley; Figure 1c); and broad, low-relief valleys with relatively little meander bend deformation (e.g., Colorado River valley; Figure 1d). We find that quantitatively, these four valley types also fall into different ranges of the valley aspect ratio ($w_v^* = (w_v - w_c)/h_c$; equation (3)). Type 1 valleys are distinguished by their narrow width relative to depth ($w_v^* < 50$). Type 2 valleys are slightly wider for the same depth ($50 \le w_v^* < 100$). Type 3 valleys ($100 \le w_v^* < 150$) have a greater median depth than type 2 valleys of the same width. Finally, type 4 valleys ($w_v^* > 150$) are widest with respect to their depth. We select quantitative bounds for these ranges based on visual inspection. The bounds separating these valley types are arbitrary, and some simulations yield topography consistent with two valley types—but the classification technique is consistent, quantitative, and reveals the major trends in valley type.

Figure 7a shows results for a phase space of simulations in E_{Vs}* and E_{Vb}*. The majority of each set of three simulations with the same parameters but different initial channel planform geometries yields a consistent valley type, but in some cases, different valley types develop because strong feedbacks between meandering

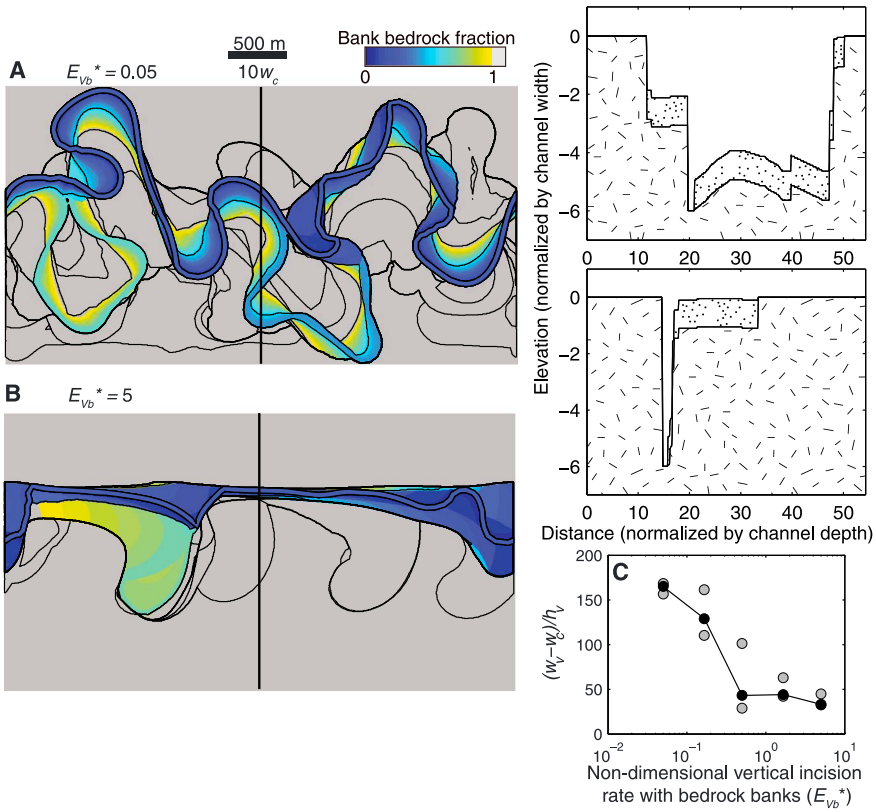

Figure 6. Valley topography formed for different values of nondimensional channel vertical erosion rate with bedrock banks, E_{Vb}^*. Symbols and coloration are the same as in Figure 3; the scale is identical in all map-view panels. All simulations use the base case parameters other than E_{Vb}^* ($t^* = 1000$, $w_{ab}^* = 0.5$, and $E_{Vs}^* = 0.005$). The mean flow direction is from left to right. Map views are shown for (a) $E_{Vb}^* = 0.05$ and (b) $E_{Vb}^* = 5$. (c) Valley aspect ratio versus E_{Vb}^* for five simulations run in triplicate with different initial channel planform geometries. The median valley aspect ratio for each value of E_{Vb}^* is shown in black.

and bank strength strongly shift the distribution of erosion across the valley. Where valley types differ within a simulation set, only two valley types occur and they fall in neighboring classification ranges of w_v^*. Differences in valley type are most strongly controlled by E_{Vb}^*. At low values of E_{Vb}^* (< 0.16), only the most expansive (types 3 and 4) valleys form, because lateral channel migration in bedrock is rapid relative to the rate of vertical incision so valley widening can keep pace with channel vertical incision even when the banks are largely bedrock. At higher values of E_{Vb}^* (> 0.16), only narrower, deeper (types 1 and 2) valleys form, because lateral channel migration in bedrock is slower relative to the rate of vertical incision. The trend of decreasing valley aspect ratio for increasing E_{Vb}^* holds for all values of E_{Vs}^*, which indicates that the ratio of channel lateral erosion in bedrock to vertical erosion is more important than the corresponding ratio for channel lateral erosion in sediment. E_{Vb}^* dictates valley aspect ratio because although the channel begins each simulation with sediment banks within the initial alluvial belt, the channel transitions to a state with a majority of all-bedrock banks except for low values of E_{Vs}^*. When E_{Vs}^* is low (0.005–0.01), channel entrenchment in bedrock is less likely, and on average, the channel can more broadly plane off the bedrock-sediment interface (e.g., Figure 5a). As a result, for fixed E_{Vb}^*, wider valleys (higher w_v^*) form at the lowest values of E_{Vs}^*. In contrast, when E_{Vs}^* is high (> 0.01), the channel bed lowers much faster than the average bedrock-sediment interface and channel evolution occurs largely with all-bedrock banks. In this case, the valley dimensions are more strongly influenced by the lower lateral erosion rate in bedrock and narrower valleys (lower w_v^*) form.

Figure 7b shows results for simulations that span a phase space in E_{Vs}^* and w_{ab}^*. In general, low values of E_{Vs}^* (≤ 0.0025) favor types 3 and 4 valleys because the rate of channel downcutting is slow with respect to lowering of the bedrock-sediment interface. For all values of vertical incision rate, valleys with larger w_v^* are

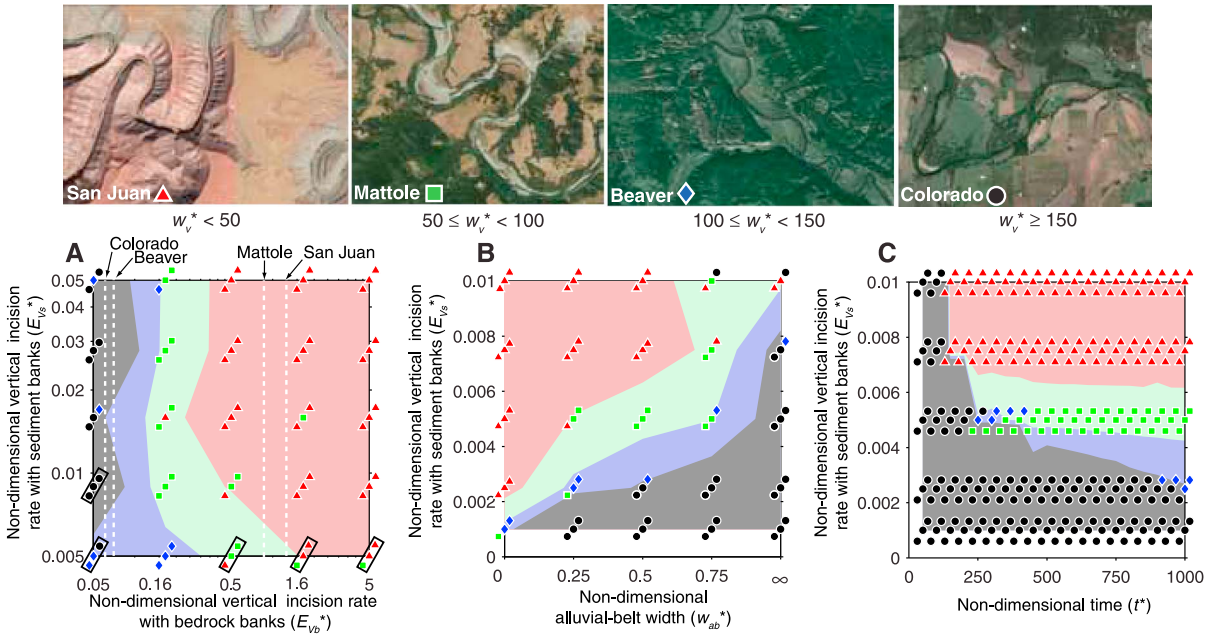

Figure 7. Model predictions for bedrock valley type, classified using valley aspect ratio (w_v^*). Each unique set of parameter values is used in three distinct simulations with different initial channel planform geometries. Each trial is plotted slightly offset from the others for legibility. For example, Figure 7a shows a 5×5 matrix of simulations in the phase space of E_{Vs}^* and E_{Vb}^*, where each unique set of parameters is plotted for three separate simulations. Valley classifications based on w_v^* are plotted for individual trials; w_v^* is averaged for each set of unique parameter values and contoured. Filled color contours indicate the classified valley types (1–4) and correspond to the representative field sites at the top of the figure. (a) Phase space of E_{Vs}^* and E_{Vb}^*. Dashed lines indicate estimated values of E_{Vb}^* for each field site. Boxes indicate simulation sets for which the majority of the channel banks are not entirely bedrock. (b) Phase space of E_{Vs}^* and w_{ab}^*. (c) Phase space of E_{Vs}^* and t^*.

favored as the degree of initial alluvial-belt confinement decreases (increasing w_{ab}^*) because the channel starts with a higher degree of mobility in sediment banks that allows it to sweep a wider valley (Figure 4). For all values of w_{ab}^*, types 1 and 2 valleys are favored as E_{Vs}^* increases because the channel cuts down faster with respect to the bedrock-sediment interface. The channel banks consequently include more bedrock, which slows valley widening. Only type 1 valleys form when there is no initial alluvial belt ($w_{ab}^* = 0$) with moderate to high vertical incision rates ($E_{Vs}^* \ge 0.0025$), because the channel begins with entirely bedrock banks and cannot erode laterally fast enough to widen the valley significantly during downcutting.

Finally, Figure 7c shows the time evolution of simulations for different values of E_{Vs}^*. In all cases, the valley evolves to a new type, and transitions to narrower, deeper valley types occur more quickly as E_{Vs}^* increases. Within each set of three simulations, the valley type at the conclusion of the simulation ($t^* = 1000$) is the same. The similarity in outcomes indicates that while the bedrock valley type observed can depend on the time, for the spin-up procedure utilized (Figure 2) the detailed sinuous channel planform geometry does not exert a strong influence on the type of valley observed at a particular time. Rather, the channel vertical incision and lateral migration rates and initial alluvial-belt width are more important in determining the valley type at $t^* = 1000$. The channel evolves from its initial state, and henceforth, the evolution of the valley type depends on the relative rates of lateral and vertical erosion and on the spatial pattern of lateral erosion guided by the alluvial-belt geometry.

5. Valley-Type Transitions by Pulses of Vertical Incision

While scenarios considered to this point have focused exclusively on cases of constant river vertical incision, a number of studies identify pulses of vertical incision as important drivers of valley-type transitions. For example, rapid vertical incision relative to lateral channel migration is the key mechanism hypothesized by *Davis* [1893] for transforming a highly sinuous alluvial channel into a bedrock-bound channel with inherited sinuosity. Pulses of vertical incision may be driven by a host of external factors, including changes in the balance of water discharge and sediment supply due to the climate change [e.g., *Hancock and Anderson*, 2002], sea level fall [e.g., *Fisk*, 1944], tectonic uplift [e.g., *Yanites et al.*, 2010], and potentially knickpoint

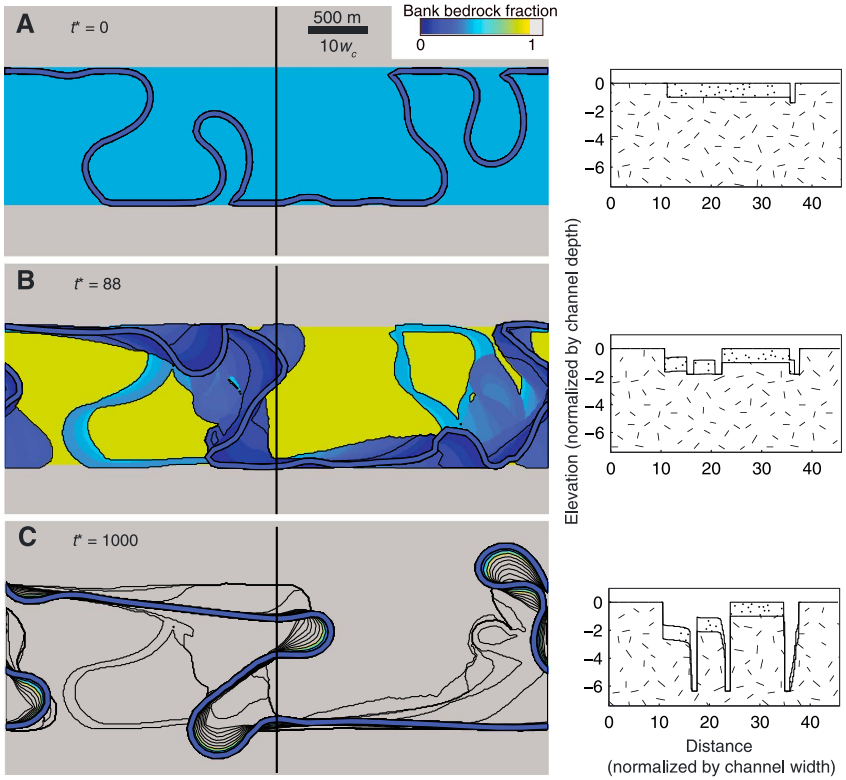

Figure 8. Valley topography during evolution from an alluvial state following a pulse of vertical incision of 0.5 h_c and constant subsequent vertical incision with $E_{Vs}^* = 0.005$. Other model parameters are set to the baseline case values ($t^* = 1000$ at the conclusion of the simulation; $E_{Vb}^* = 0.5$; and $w_{ab}^* = 0.5$). Symbols and coloration are the same as in Figure 3; the scale is identical in all map-view panels and the mean flow direction is from left to right. (a) $t^* = 0$; (b) $t^* = 88$ (as in Figure 3c of the baseline case); (c) $t^* = 1000$ (as in Figure 3g of the baseline case).

propagation following meander cutoff [*Finnegan and Dietrich*, 2011]. Here we relax the assumption of constant vertical incision employed in the simulations in section 4 by comparison to example cases with pulses of vertical incision.

We first consider the effect of a vertical incision pulse less than the channel depth. We initialize a simulation with a partially confined meander-belt equivalent to the baseline case ($w_{ab}^* = 0.5$), i.e., the channel is inset in alluvium with depth equal to the channel depth, with bedrock below and on the lateral margins of this sediment cover, and other model parameters ($E_{Vb}^* = 0.5$ and $t^* = 1000$) are equal to those in the baseline case. In this case, however, the channel also undergoes a spatially uniform pulse of vertical incision of 0.5 h_c at the start of the simulation, which establishes a bank bedrock fraction of 0.5 throughout the model domain (Figure 8a). At $t^* = 88$ (Figure 8b), the channel maintains high sinuosity in a zone of low bank bedrock fraction within the boundaries of the initial alluvial belt, similar to the corresponding time step for the baseline case with no vertical incision pulse (Figure 3c). At $t^* = 1000$ (Figure 8c), in most places, the channel has extremely low sinuosity at short wavelengths (≤ 15 w_c) because it lost sinuosity in a manner similar to the baseline case (Figure 3g), and similarly, the channel is entrenched in all-bedrock banks. These similarities with the baseline case suggest that pulses of vertical incision—and by extension, changes in external forcing—must exceed a threshold in order to affect valley type.

In Figure 9, we simulate the response of a valley following an incision pulse equal to the channel depth for cases with relatively rapid ($E_{Vb}^* = 0.5$; Figure 9a) and relatively slow subsequent vertical channel incision ($E_{Vb}^* = 0.05$; Figure 9b). Other model parameters ($t^* = 1000$; $w_{ab}^* = 0.5$) are equal to those in Figure 8 and the baseline case, except E_{Vs}^* which covaries with E_{Vb}^* in this case. The simulations show that following the vertical incision pulse, the persistence of the sinuous channel's bedrock-bound state depends on the vertical incision rate. When the vertical incision rate is high, after the initial incision pulse, the channel forms slip-off

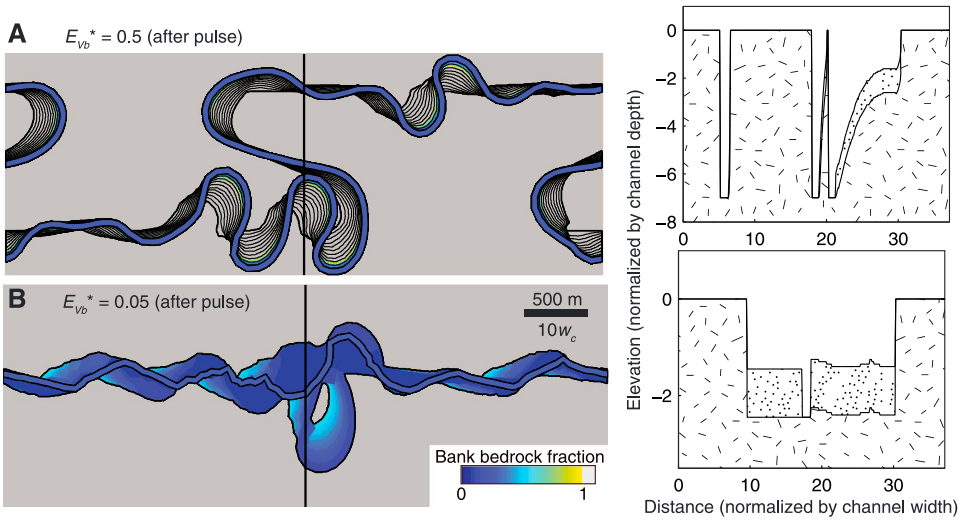

Figure 9. Valley topography during evolution from an alluvial state following a pulse of vertical incision of h_c, larger than the pulse in Figure 9. Other model parameters are set to the baseline case values (t^* = 1000 and w_{ab}^* = 0.5). Symbols and coloration are the same as in Figure 3; the scale is identical in both map-view panels and the mean flow direction is from left to right. (a) Pulse of vertical incision is followed by constant, relatively rapid vertical incision with E_{Vs}^* = 0.005. (b) Pulse of vertical incision is followed by constant, relatively slow vertical incision with E_{Vs}^* = 0.0005.

surfaces along the inside of meander bends (Figure 9a), but the cutbanks along growing bends are entirely bedrock. In contrast, in the baseline case with no incision pulse (Figure 3), terraces near the channel level illustrate that the valley took longer to reach a bedrock-entrenched state. Under a low vertical incision rate following the incision pulse, channel lateral migration is able to widen the valley quickly enough to form a continuous zone of largely sediment fill in which the channel is more mobile (Figure 9b). The final alluvial-belt width is wider than in the baseline case (Figure 3g). The different states of the two valleys that have undergone pulses of vertical incision show that while the bedrock-entrenched channel state at the start of the simulation is genetically related to the vertical incision pulse, the preservation of this geomorphic signal depends on the subsequent evolution of the channel under steady forcing.

6. Comparison to Natural River Valleys

To relate the model results to natural bedrock river valleys, we compare the valleys introduced in Figure 1 to summary model predictions for constant vertical incision cases. Because of the difficulty of reconstructing the initial alluvial-belt width of the channel, we focus the comparison on model predictions that fix the nondimensional alluvial-belt width but vary the vertical erosion rate and the lateral erosion rates in bedrock and sediment (Figure 7a). We begin this section by briefly introducing the key attributes of four field sites that correspond to model inputs (Table 2). While all field sites may have undergone changes in climate and base level that could influence their present valley type, here as in section 4, we restrict our analysis to a constant-forcing framework that serves as a null hypothesis to more complex scenarios. Each river valley may have developed over longer timescales, but we compare each valley to model data with a dimensional simulation time of t = 25 kyr in order to test whether the constant-input model can reproduce the general valley types represented by each field case. Lateral migration rates for meandering rivers vary in space [*Hickin and Nanson*, 1975; *Hudson and Kesel*, 2000], and the meandering model employed yields a maximum migration

Table 2. Estimated Parameters for Field Sites Shown in Figures 1 and 7

Valley Name	w_c (m)	h_c (m)	E_{Lb} (m/yr)	E_V (mm/yr)	E_{Vb}^*
San Juan	53	2.1	0.003	0.15	1.26
Mattole	102	4	0.03	1	0.86
Beaver	44	1.8	0.035	0.1	0.07
Colorado	275	8	0.15	0.25	0.06

rate approximately 3 times faster than the mean. Therefore, where constraints for lateral erosion rate are available, they are assumed to be mean rates and are converted to maximum rates (E_{Lb} and E_{Ls}) by multiplying by a factor of 3.

The *San Juan River* (southern Utah) is one of many sinuous channels incised in bedrock in the Colorado Plateau [*Harden*, 1990]. Geochronology data indicate a vertical incision rate of 0.11–0.21 mm/yr in the region averaged over the last several hundred thousand years [*Pederson et al*., 2002; *Wolkowinsky and Granger*, 2004; *Hanks and Finkel*, 2005]. Lateral erosion rate measurements are unavailable for the San Juan River and are generally scarce for similar bedrock-bound rivers, but we estimate that the bedrock lateral erosion rate is an order of magnitude slower than rates of ~1 cm/yr estimated for rivers eroding weaker sedimentary rock [e.g., *Montgomery*, 2004; *Fuller et al*., 2009; *Finnegan and Dietrich*, 2011]. Taking 1 mm/yr as a mean lateral erosion rate in bedrock, this yields $E_{Lb} = 3$ mm/yr. From the average of 10 spot measurements in air photos, we estimate $w_c = 53$ m (bankfull) near Mexican Hat, Utah, and $h_c = 2.1$ m (assuming $w_c/h_c = 25$).

The *Mattole River* traverses a tectonically active region in coastal northern California. Dated strath terraces constrain the river vertical incision rate to 0.7–1.8 mm/yr over the last 12 kyr near Honeydew, CA [*Merritts et al*., 1994]. *Merritts et al*. [1994] argued that the Mattole's strath terraces—subparallel, closely spaced in elevation, unpaired, and with similar gradients to adjacent channel reaches—formed by channel wandering with constant vertical incision. The lateral erosion rate in bedrock has been estimated at 13 mm/yr for the Eel River, California [*Fuller et al*., 2009] and 6 mm/yr along the Smith River, Oregon [*Finnegan and Dietrich*, 2011], which also incise predominantly weak, fine-grained sedimentary rocks in similar climatic and tectonic settings. Based on these constraints, we estimate a mean lateral erosion rate in bedrock of 10 mm/yr ($E_{Lb} = 30$ mm/yr) and $E_V = 1$ mm/yr. We estimate $w_c = 102$ m (bankfull) based on 10 spot measurements in air photos near Honeydew, CA, and $h_c = 4.1$ m (assuming $w_c/h_c = 25$).

The *Beaver River* crosses the plains east of the Canadian Rockies and regularly meets its valley walls at large angles [*Carson and Lapointe*, 1983; *Nicoll and Hickin*, 2010]. The long wavelength of the valley walls compared to the active meanders has been inferred to reflect a decrease in discharge following deglaciation [*Dury*, 1964]. *Nicoll and Hickin* [2010] reported a 3.5 m/yr maximum lateral erosion rate over a 48 year interval based on air photo analysis. The regularity of meander geometry suggests that down-valley bend translation occurs much faster than valley widening [*Parker et al*., 1983], which we estimate as 2 orders of magnitude less than the maximum channel lateral erosion rate (3.5 cm/yr). Because the valley walls are alluvium rather than consolidated bedrock, the valley widening rate substitutes for E_{Lb} in the model framework. The channel width (h_c) is 44 m [*Nicoll and Hickin*, 2010] and we estimate $h_c = 1.8$ m (assuming $w_c/h_c = 25$). Based on the continental interior setting and lack of prominent terraces, we estimate $E_V = 0.1$ mm/yr.

The *Colorado River (Texas)* flows through a low-relief valley composed of weak sedimentary bedrock, with a mixed bedrock-alluvial bed, between Austin and Columbus [*Baker*, 1977; *Baker and Penteado-Orellana*, 1977; *Blum and Aslan*, 2006]. Meandering rivers in the region have abandoned a series of strath terraces that extend inland ~250 km from the coast [*Baker and Penteado-Orellana*, 1977; *Blum and Valastro*, 1994]. Meanders throughout the Texas outer coastal plain evolve significantly on an annual timescale, with channel migration rates of several meters per year [e.g., *Wellmeyer et al*., 2005], but channel migration likely proceeds more slowly for inner coastal plain meanders incised in bedrock [*Stricklin*, 1961]. Based on stratigraphic data [*Baker and Penteado-Orellana*, 1977; *Blum and Valastro*, 1994], we estimate $E_{Lb} = 5$ cm/yr and $E_V = 0.25$ mm/yr over the last 20 kyr. Cross-section data from Austin indicate $w_c = 275$ m and $h_c = 8$ m for a 2 year flood before damming [*Blum*, 1992], which are taken as the bankfull dimensions.

Among the chosen field sites, only the Beaver River actively migrates in sediment banks, so we estimate E_{Vb}^* for each river (Table 2) and compare these values to model predictions for valley type in Figure 7a. The estimated values of E_{Vb}^* are relatively low for Colorado River and Beaver River, and this portion of the model phase space uniformly predicts the formation of relatively broad and shallow (types 3 and 4) valleys. Similarly, the estimated values of E_{Vb}^* are relatively high for the Mattole and San Juan Rivers and correspond to a portion of phase space dominated by narrow and deep (largely type 1) valleys. These results suggest that the constant vertical erosion framework can reproduce the general trends in valley aspect ratio for the field sites, even without knowledge of the lateral erosion rate each river would exhibit in sediment banks. This result is consistent with E_{Vb}^* operating as a key driver of valley type (Figure 7a). Importantly, pulses of vertical incision

are not required to explain the trend in valley aspect ratio for the field sites, implying that valley aspect ratio may not be a diagnostic indicator of vertical incision history.

7. Discussion

The modest number of independent variables explored here—channel lateral migration rates in sediment and bedrock, vertical erosion rate, and initial alluvial-belt width—can account for a wide range of observed bedrock valley types (Figure 7) that cannot be reproduced without accounting for bank strength differences. In particular, without bank strength differences, the model can produce bedrock-bound meanders [e.g., *Finnegan and Dietrich*, 2011] and broad alluvial plains [e.g., *Howard*, 1996] like the San Juan and Colorado River valleys, respectively; but it cannot produce meander bends that deform against valley walls nor confined alluvial belts, as occur in the Beaver and Mattole River valleys. Such bend deformation only occurs when a factor external to the channel locally slows channel migration with respect to neighboring reaches. Simulations confirm the central hypothesis that the coevolution of channel lateral migration and bank strength under a constant vertical incision rate can determine the first-order geometry of bedrock river valleys.

Simulation results that span a range of channel lateral migration rates in sediment and bedrock, vertical incision rates, and initial alluvial widths (Figure 7) allow reassessment of the hypotheses for bedrock river valley evolution posed in section 1. We revisit whether valley type can be used to differentiate river vertical incision scenarios, and whether valley types can be formed without abrupt pulses of vertical incision. In contrast, an alternate view is that particular bedrock valley types, and in particular deep, narrow valleys with sinuous channels or those with strath terraces, require pulses of vertical incision to form [e.g., *Gilbert*, 1877; *Davis*, 1893; *Hancock and Anderson*, 2002; *Pan et al*., 2003; *Finnegan and Dietrich*, 2011]. Simulations presented here suggest that a range of river vertical incision rates can result in an initially alluvial-banked channel becoming entrenched into bedrock (Figure 7). Moreover, simulations indicate that channel entrenchment may arise not solely through high rates of vertical incision and low rates of channel lateral migration in bedrock but also by interplay between channel lateral migration in sediment and vertical incision that determines the ability of the channel to maintain a zone of sediment fill within the valley.

Counterintuitively, the channel is most effective at maintaining an alluvial channel belt when bedrock boundaries constrain the range of lateral channel migration (Figure 4b). On one hand, channels can move rapidly in alluvium and develop high sinuosity, which reinforces high lateral erosion rates, including for local zones of bedrock banks. On the other hand, the bedrock constraints focus planation of the sediment-bedrock interface to a relatively narrow zone, which forces valley floor lowering to keep pace with channel vertical incision. Without a bedrock constraint at the margins of the alluvial belt (Figure 4c), lateral channel migration is spread over a relatively broad zone, which causes the sediment-bedrock interface to lower more slowly than the vertically incising channel and leads to channel entrenchment in bedrock. This behavior suggests that even when alluvium only mantles a bedrock river valley, it plays an important role in valley evolution because it determines the width of the valley floor that the channel can actively migrate across and plane off the sediment-bedrock interface (e.g., Figure 5).

The existence of a laterally constrained alluvial belt also influences the planform sinuosity of the valley boundaries. Our simulations show that for a fixed channel geometry and wavelength of unconfined meandering, channel migration in a confined alluvial belt results in erosional arcuate scars in the valley walls that have a range of wavelengths. Large contrasts in bedrock versus sediment bank strength favor scars with wavelengths longer than the typical channel wavelength for unconfined meandering ($> 15\ w_c$; Figure 6), a pattern widely observed in natural, "underfit" river valleys [*Dury*, 1964]. In the simulations, the long-wavelength valley scars form by meander bend deformation at the alluvial-belt boundaries [*Lewin and Brindle*, 1977], but also through progressive sculpting by wall-parallel channel migration (Figure 4b and supporting information Movie S2). Meander wavelength is well established to scale with channel width and discharge in alluvial rivers [e.g., *Leopold and Wolman*, 1960; *Williams*, 1986], and so meander scars in valley walls have been interpreted as evidence of higher paleodischarge [e.g., *Dury*, 1964, 1985; *Baker and Penteado-Orellana*, 1977; *Alford and Holmes*, 1985]. Our results instead suggest that eroded forms in valley walls do not directly record paleochannel dimensions because meander bend deformation and migration parallel to the valley walls generates scars with wavelengths longer than the typical channel wavelength

for free meandering. Therefore, paleochannel deposits [e.g., *Leigh and Feeney*, 1995] may be more reliable indicators of channel dimensions.

The result that bedrock-bound channels can evolve under steady forcing from alluvial states leads to the broader question of whether, in general, multiple kinematic paths can lead to a particular bedrock river valley type. Simulations indicate that several bedrock valley types can arise from one of the other bedrock valley types (Figure 7). Of particular interest is the emergent development of valleys in which meander bends deform at the alluvial-belt boundaries (Figures 1c and 4b and supporting information Movie S2), as suggested by earlier studies that did not include channel vertical incision [*Howard*, 1996; *Sun et al*., 1996]. The broader significance of this finding is that the evolution of bank strength accounted for in the present model and suggested in previous work [*Howard*, 1996; *Sun et al*., 1996] allows for valley states to arise naturally from other states without being directly imposed by initial conditions. Using the nondimensional variables E_{Vb}*, E_{Vs}*, and w_{ab}*, there are zones of phase space in which particular valley types are likely to emerge, and other zones that may yield multiple valley types (Figure 7).

While channel lateral migration rate, vertical incision rate, and bank strength have been suggested as important controls on valley type [e.g., *Harden*, 1990; *Merritts et al*., 1994; *Hancock and Anderson*, 2002; *Montgomery*, 2004], their combined influences have not been tested quantitatively in previous models. Results here suggest that (1) channel lateral migration rates in bedrock and sediment, (2) vertical incision rate, and (3) the width of the initial alluvial belt with respect to the potential width of the unconfined alluvial belt can each strongly influence valley evolution; no single factor overwhelms the others. As suggested by *Montgomery* [2004], bedrock erodibility can explain differences in bedrock valley type, with weaker bedrock favoring formation of relatively wide valleys across a range of river vertical incision rates. Low channel lateral migration rates and high vertical incision rates generally favor narrow valleys, while high lateral migration rates and low vertical incision rates favor wide valleys. While past valley topography and alluvial-belt width are difficult to constrain, particularly over landscape evolution timescales of $\geq 10^5$ years, forward modeling can explore the implications of different hypotheses for former valley characteristics.

The simulation results can also address whether the different valley types observed in nature are stable under steady forcing, or whether aspects of their geometry may be transient. We find that some portions of the explored parameter space are likely stable: for example, narrow and deep valleys, and broad and shallow valleys can remain stable because channel vertical incision rates are either high enough to keep channels persistently entrenched in bedrock or low enough to allow channel lateral migration to widely bevel the bedrock-sediment interface and maintain alluvial banks (Figures 7a and 7b). There are, however, ranges of lateral migration and vertical incision rates and initial alluvial-belt widths that permit evolution through transient valley types (Figure 7c). In the intermediate ranges of E_{Vb}*, E_{Vs}*, and w_{ab}*, transitions between different valley types can be driven by the inherent unsteadyness of lateral channel migration, which can cause different valley topography despite similar process rates (Figure 7). Therefore, the statistical behavior of a set of simulations may be needed to identify links between environmental drivers and valley evolution and to characterize uncertainty in simulation results [e.g., *Griffiths*, 1982; *Nicholas and Quine*, 2010; *Perron and Fagherazzi*, 2012]. While constant vertical incision can drive transitions between valley type, we also find that valley type may be unaffected by pulses of vertical incision as large as 0.5 channel depths (Figure 9). This suggests a threshold on the magnitude of climate and base-level signals that can be preserved in bedrock valley topography.

Changes in base level, sediment supply, and water discharge are widely implicated as drivers of time-varying river vertical incision rates, which are the commonly argued prerequisite to strath terrace formation [e.g., *Gilbert*, 1877; *Hancock and Anderson*, 2002; *Wegmann and Pazzaglia*, 2002; *Pan et al*., 2003; *Fuller et al*., 2009]. The numerical model of *Hancock and Anderson* [2002] illustrates this concept but importantly utilizes a one-dimensional framework with a consistent direction of valley widening that cannot generate terraces by changes in channel migration direction under constant vertical incision rates. The simulations presented here, which incorporate two-dimensional channel meandering, show that the intrinsic unsteadiness of meander migration in space and time, coupled with a constant vertical incision rate, can generate strath terraces without pulses of incision. These terraces are commonly unpaired (Figure 6), as which has been argued to indicate formation by intrinsic processes [e.g., *Merritts et al*., 1994]. Yet paired terraces also form (Figure 5b), and this geometry is commonly suggested to implicate external drivers of channel evolution [e.g., *Wegmann and Pazzaglia*, 2002], which is not the case in our simulations.

Our simulations suggest more broadly that constant-forcing scenarios that account for unsteady channel lateral channel migration represent an important null hypothesis for valley evolution. Since a variety of bedrock valley types can be explained without pulses of vertical incision, valley aspect ratio may not diagnostically identify valleys that have undergone externally forced pulses of vertical incision. Other morphologic evidence may distinguish constant from pulsed vertical incision histories—for example, in the simulations bedrock-bound channels that evolve from initial states with sediment banks (Figure 3g) exhibit low sinuosity at short wavelengths ($\leq 15\ w_c$) compared to bedrock-bound channels that do not lose sinuosity during a transient alluvial phase (Figure 9a). Alternatively, geochronology can offer more direct constraints on vertical incision history, however, even here inferring the degree to which river incision is unsteady is not straightforward [*Finnegan et al*., 2014].

8. Conclusions

We present a model, based on interactions between channel lateral migration and vertical incision, that can reproduce a wide spectrum of bedrock valleys with single-thread meandering channels. We identify the channel vertical incision rate, lateral migration rates in sediment and bedrock, and initial alluvial-belt width as key controls on valley type. Despite these first-order trends, model results indicate that valley types can be unstable under steady forcing and that different valley types can arise from multiple evolutionary pathways. Bedrock-bound channels, strath terraces, and valley scars with wavelengths longer than the free meander wavelength all arise under constant forcing, further suggesting that unsteady lateral channel migration due to meandering should be considered as a null hypothesis for valley evolution. Bank strength differences between sediment and bedrock reinforce irregularity in meandering in space and time, and sustained planation of the valley floor is enhanced when lateral bedrock boundaries focus the zone of lateral channel migration in sediment banks. Finally, the persistence of channel entrenchment in bedrock following a rapid pulse of vertical incision depends on subsequent rates of channel lateral migration and vertical incision, suggesting that bedrock river valley topography is a useful but potentially transient marker of environmental and tectonic signals.

Acknowledgments
This work was supported by the Department of Defense through the National Defense Science and Engineering Graduate Fellowship (NDSEG) Program and NSF grant EAR-1147381 to MPL. Acknowledgment is also made to the Donors of the American Chemical Society Petroleum Research Fund for partial support of this research. We thank Jean-Philippe Avouac, Noah Finnegan, Alan Howard, Bob Anderson, Brian Yanites, and Associate Editor Dimitri Lague for helpful comments.

References

Alford, J. J., and J. C. Holmes (1985), Meander scars as evidence of major climate change in southwest Louisiana, *Ann. Assoc. Am. Geogr.*, *75*(3), 395–403, doi:10.1111/j.1467-8306.1985.tb00074.x.
Amos, C. B., and D. W. Burbank (2007), Channel width response to differential uplift, *J. Geophys. Res.*, *112*, F02010, doi:10.1029/2006JF000672.
Baker, V. R. (1977), Stream-channel response to floods, with examples from central Texas, *Geol. Soc. Am. Bull.*, *88*(8), 1057–1071, doi:10.1130/0016-7606(1977)88<1057:SRTFWE>2.0.CO;2.
Baker, V. R. (2001), Water and the Martian landscape, *Nature*, *412*(6843), 228–236, doi:10.1038/35084172.
Baker, V. R., and M. M. Penteado-Orellana (1977), Adjustment to Quaternary climatic change by the Colorado River in central Texas, *J. Geol.*, *85*(4), 395–422.
Barbour, J. R. (2008), The origin and significance of sinuosity along incising bedrock rivers, PhD thesis, Columbia University, New York, N. Y.
Blum, M. D. (1992), Modern depositional environments and recent alluvial History of the lower Colorado River, Gulf coastal plain of Texas, PhD thesis, Univ. Texas at Austin, Austin, Tex.
Blum, M. D., and A. Aslan (2006), Signatures of climate vs. sea-level change within incised valley-fill successions: Quaternary examples from the Texas Gulf coast, *Sediment. Geol.*, *190*(1–4), 177–211, doi:10.1016/j.sedgeo.2006.05.024.
Blum, M. D., and T. E. Tornqvist (2000), Fluvial responses to climate and sea-level change: A review and look forward, *Sedimentology*, *47*, 2–48, doi:10.1046/j.1365-3091.2000.00008.x.
Blum, M. D., and S. Valastro (1994), Late Quaternary sedimentation, lower Colorado River, Gulf coastal-plain, *Geol. Soc. Am. Bull.*, *106*(8), 1002–1016, doi:10.1130/0016-7606(1994)106<1002:LQSLCR>2.3.CO;2.
Braun, J., and M. Sambridge (1997), Modelling landscape evolution on geological time scales: A new method based on irregular spatial discretization, *Basin Res.*, *9*(1), 27–52, doi:10.1046/j.1365-2117.1997.00030.x.
Burr, D. M., et al. (2013), Fluvial features on Titan: Insights from morphology and modeling, *Geol. Soc. Am. Bull.*, *125*(3–4), 299–321.
Camporeale, C., P. Perona, A. Porporato, and L. Ridolfi (2005), On the long-term behavior of meandering rivers, *Water Resour. Res.*, *41*, W12403, doi:10.1029/2005WR004109.
Carson, M. A., and M. F. Lapointe (1983), The inherent asymmetry of river meander planform, *J. Geol.*, *91*(1), 41–55.
Cook, K. L., K. X. Whipple, A. M. Heimsath, and T. C. Hanks (2009), Rapid incision of the Colorado River in Glen Canyon - Insights from channel profiles, local incision rates, and modeling of lithologic controls, *Earth Surf. Processes Landforms*, *34*, 994–1010, doi:10.1002/esp.1790.
Davis, W. M. (1893), The topographic maps of the United States Geological Survey, *Science*, *21*(534), 225–227.
Dury, G. (1985), Attainable standards of accuracy in the retrodiction of paleodischarge from channel dimensions, *Earth Surf. Processes Landforms*, *10*(3), 205–213, doi:10.1002/esp.3290100303.
Dury, G. H. (1964), Principles of underfit streams, Professional Paper 452-A, US Geological Survey.
Ferguson, R. I. (1973), Channel pattern and sediment type, *Area*, *5*, 38–41.
Finnegan, N. J., and G. Balco (2013), Sediment supply, base level, braiding, and bedrock river terrace formation: Arroyo Seco, California, USA, *Geol. Soc. Am. Bull.*, *125*(7–8), 1114–1124, doi:10.1130/B30727.1.

Finnegan, N. J., and W. E. Dietrich (2011), Episodic bedrock strath terrace formation due to meander migration and cutoff, *Geology*, *39*(2), 143–146, doi:10.1130/G31716.1.
Finnegan, N. J., G. Roe, D. R. Montgomery, and B. Hallet (2005), Controls on the channel width of rivers: Implications for modeling fluvial incision of bedrock, *Geology*, *33*(3), 229–232, doi:10.1130/G21171.1.
Finnegan, N. J., R. Schumer, and S. Finnegan (2014), A signature of transience in bedrock river incision rates over timescales of 104–107 years, *Nature*, *505*(7483), 391–394, doi:10.1038/nature12913.
Fisk, H. N. (1944), *Geological Investigation of the Alluvial Valley of the Lower Mississippi River*, Mississippi River Commission, Vicksburg.
Frascati, A., and S. Lanzoni (2010), Long-term river meandering as a part of chaotic dynamics? A contribution from mathematical modelling, *Earth Surf. Processes Landforms*, *35*(7), 791–802, doi:10.1002/esp.1974.
Fuller, T. K., L. A. Perg, J. K. Willenbring, and K. Lepper (2009), Field evidence for climate-driven changes in sediment supply leading to strath terrace formation, *Geology*, *37*(5), 467–470, doi:10.1130/G25487A.1.
Gilbert, G. K. (1877), *Report on the Geology of the Henry Mountains*, US Government Printing Office, Washington, D. C.
Griffiths, G. A. (1982), Stochastic prediction in geomorphology using Bayesian inference models, *Math. Geol.*, *14*(1), 65–75, doi:10.1007/BF01037448.
Hancock, G. S., and R. S. Anderson (2002), Numerical modeling of fluvial strath-terrace formation in response to oscillating climate, *Geol. Soc. Am. Bull.*, *114*(9), 1131–1142.
Hanks, T. C., and R. C. Finkel (2005), Early Pleistocene incision of the San Juan River, Utah, dated with 26Al and 10Be: Comment and Reply COMMENT, *Geology*, *33*(1), e78–e79, doi:10.1130/0091-7613-33.1.e78.
Harden, D. (1990), Controlling factors in the distribution and development of incised meanders in the central Colorado Plateau, *Geol. Soc. Am. Bull.*, *102*(2), 233–242, doi:10.1130/0016-7606(1990)102<0233:CFITDA>2.3.CO;2.
Hartshorn, K., N. Hovius, W. B. Dade, and R. L. Slingerland (2002), Climate-driven bedrock incision in an active mountain belt, *Science*, *297*(5589), 2036–2038, doi:10.1126/science.1075078.
Hickin, E. J., and G. C. Nanson (1975), The character of channel migration on the Beatton River, northeast British Columbia, Canada, *Geol. Soc. Am. Bull.*, *86*(4), 487–494, doi:10.1130/0016-7606(1975)86<487:TCOCMO>2.0.CO;2.
Howard, A., and A. Hemberger (1991), Multivariate characterization of meandering, *Geomorphology*, *4*(3–4), 161–186, doi:10.1016/0169-555X(91)90002-R.
Howard, A. D. (1992), Modeling channel migration and floodplain sedimentation in meandering streams, in *Lowland Floodplain Rivers: Geomorphological Perspectives*, edited by P. A. Carling and G. E. Petts, pp. 1–41, John Wiley, Chichester.
Howard, A. D. (1996), Modelling channel evolution and floodplain morphology, in *Floodplain Processes*, edited by M. G. Anderson, D. E. Walling, and P. E. Bates, pp. 15–62, John Wiley, Chichester.
Howard, A. D., and T. R. Knutson (1984), Sufficient conditions for river meandering—A simulation approach, *Water Resour. Res.*, *20*(11), 1659–1667, doi:10.1029/WR020i011p01659.
Howard, A. D., W. E. Dietrich, and M. A. Seidl (1994), Modeling fluvial erosion on regional to continental scales, *J. Geophys. Res.*, *99*(B7), 13,971–13,986, doi:10.1029/94JB00744.
Hudson, P. F., and R. H. Kesel (2000), Channel migration and meander-bend curvature in the lower Mississippi River prior to major human modification, *Geology*, *28*(6), 531–534, doi:10.1130/0091-7613(2000)28<531:CMAMCI>2.0.CO;2.
Ikeda, S., G. Parker, and K. Sawai (1981), Bend theory of river meanders. Part 1. Linear development, *J. Fluid Mech.*, *112*(11), 363–377.
Lague, D. (2010), Reduction of long-term bedrock incision efficiency by short-term alluvial cover intermittency, *J. Geophys. Res.*, *115*, F02011, doi:10.1029/2008JF001210.
Lancaster, S. T. (1998), A nonlinear river meandering model and its incorporation in a landscape evolution model, PhD thesis, Massachusetts Institute of Technology, Cambridge, Mass.
Lavé, J., and J. P. Avouac (2000), Active folding of fluvial terraces across the Siwaliks Hills, Himalayas of central Nepal, *J. Geophys. Res.*, *105*(B3), 5735–5770, doi:10.1029/1999JB900292.
Lavé, J., and J. P. Avouac (2001), Fluvial incision and tectonic uplift across the Himalayas of central Nepal, *J. Geophys. Res.*, *106*(B11), 26,561–26,591, doi:10.1029/2001JB000359.
Leigh, D. S., and T. P. Feeney (1995), Paleochannels indicating wet climate and lack of response to lower sea level, southeast Georgia, *Geology*, *23*(8), 687–690, doi:10.1130/0091-7613(1995)023<0687:PIWCAL>2.3.CO;2.
Leopold, L. B., and M. G. Wolman (1960), River meanders, *Geol. Soc. Am. Bull.*, *71*(6), 769–793, doi:10.1130/0016-7606(1960)71[769:RM]2.0.CO;2.
Lewin, J., and B. J. Brindle (1977), Confined meanders, in *River Channel Changes*, edited by K. J. Gregory, pp. 221–233, John Wiley, Chichester.
Limaye, A. B. S., and M. P. Lamb (2013), A vector-based method for bank-material tracking in coupled models of meandering and landscape evolution, *J. Geophys. Res. Earth Surf.*, *118*, 2421–2437, doi:10.1002/2013JF002854.
Merritts, D. J., K. R. Vincent, and E. E. Wohl (1994), Long river profiles, tectonism, and eustasy - A guide to interpreting fluvial terraces, *J. Geophys. Res.*, *99*(B7), 14,031–14,050, doi:10.1029/94JB00857.
Molnar, P., E. T. Brown, B. C. Burchfiel, Q. Deng, X. Feng, J. Li, G. M. Raisbeck, J. Shi, W. Zhangming, and F. Yiou (1994), Quaternary climate change and the formation of river terraces across growing anticlines on the north flank of the Tien Shan, China, *J. Geol.*, *102*(5), 583–602.
Montgomery, D. R. (2004), Observations on the role of lithology in strath terrace formation and bedrock channel width, *Am. J. Sci.*, *304*(5), 454–476, doi:10.2475/ajs.304.5.454.
Nanson, G. C., and E. J. Hickin (1986), A statistical analysis of bank erosion and channel migration in western Canada, *Geol. Soc. Am. Bull.*, *97*(4), 497–504, doi:10.1130/0016-7606(1986)97<497:ASAOBE>2.0.CO;2.
Nicholas, A. P., and T. A. Quine (2010), Quantitative assessment of landform equifinality and palaeoenvironmental reconstruction using geomorphic models, *Geomorphology*, *121*(3–4), 167–183, doi:10.1016/j.geomorph.2010.04.004.
Nicoll, T. J., and E. J. Hickin (2010), Planform geometry and channel migration of confined meandering rivers on the Canadian prairies, *Geomorphology*, *116*(1–2), 37–47, doi:10.1016/j.geomorph.2009.10.005.
Pan, B., D. Burbank, Y. Wang, G. Wu, J. Li, and Q. Guan (2003), A 900 k.y. record of strath terrace formation during glacial-interglacial transitions in northwest China, *Geology*, *31*(11), 957–960, doi:10.1130/G19685.1.
Parker, G. (1976), On the cause and characteristic scales of meandering and braiding in rivers, *J. Fluid Mech.*, *76*(3), 457–480, doi:10.1017/S0022112076000748.
Parker, G., P. Diplas, and J. Akiyama (1983), Meander bends of high amplitude, *J. Hydraul. Eng.*, *109*(10), 1323–1337, doi:10.1061/(ASCE)0733-9429(1983)109:10(1323.
Parker, G., Y. Shimizu, G. V. Wilkerson, E. C. Eke, J. D. Abad, J. W. Lauer, C. Paola, W. E. Dietrich, and V. R. Voller (2011), A new framework for modeling the migration of meandering rivers, *Earth Surf. Processes Landforms*, *36*(1), 70–86, doi:10.1002/esp.2113.

Pederson, J., K. Karlstrom, W. Sharp, and W. McIntosh (2002), Differential incision of the Grand Canyon related to Quaternary faulting—Constraints from U-series and Ar/Ar dating, *Geology*, *30*(8), 739–742.

Perron, J. T., and S. Fagherazzi (2012), The legacy of initial conditions in landscape evolution, *Earth Surf. Processes Landforms*, *37*(1), 52–63, doi:10.1002/esp.2205.

Seidl, M. A., and W. E. Dietrich (1992), The problem of channel erosion into bedrock, *Catena Suppl.*, *23*, 101–124.

Seminara, G. (2006), Meanders, *J. Fluid Mech.*, *554*(1), 271–297, doi:10.1017/S0022112006008925.

Shyu, J. B. H., K. Sieh, J.-P. Avouac, W.-S. Chen, and Y.-G. Chen (2006), Millennial slip rate of the Longitudinal Valley fault from river terraces: Implications for convergence across the active suture of eastern Taiwan, *J. Geophys. Res.*, *111*, B08403, doi:10.1029/2005JB003971.

Sklar, L. S., and W. E. Dietrich (2001), Sediment and rock strength controls on river incision into bedrock, *Geology*, *29*(12), 1087–1090, doi:10.1130/0091-7613(2001)029<1087:SARSCO>2.0.CO;2.

Stark, C. P. (2006), A self-regulating model of bedrock river channel geometry, *Geophys. Res. Lett.*, *33*, L04402, doi:10.1029/2005GL023193.

Stark, C. P., J. R. Barbour, Y. S. Hayakawa, T. Hattanji, N. Hovius, H. Chen, C.-W. Lin, M.-J. Horng, K.-Q. Xu, and Y. Fukahata (2010), The climatic signature of incised river meanders, *Science*, *327*(5972), 1497–1501, doi:10.1126/science.1184406.

Stølum, H.-H. (1996), River meandering as a self-organization process, *Science*, *271*(5256), 1710–1713, doi:10.1126/science.271.5256.1710.

Stricklin, F. L. (1961), Degradational stream deposits of the Brazos River, central Texas, *Geol. Soc. Am. Bull.*, *72*(1), 19–36.

Sun, T., P. Meakin, T. Jossang, and K. Schwarz (1996), A simulation model for meandering rivers, *Geophys. Res. Lett.*, *32*(9), 2937–2954, doi:10.1029/96WR00998.

Tinkler, J., and E. Wohl (1998), *Rivers Over Rock: Fluvial Processes in Bedrock Channels*, *Geophysical Monograph Series*, AGU, Washington, D. C.

Tucker, G. E., S. T. Lancaster, N. M. Gasparini, and R. L. Bras (2001), The channel-hillslope integrated landscape development model (CHILD), in *Landscape Erosion and Evolution Modeling*, edited by R. S. Harmon and W. W. Doe III, pp. 349–388, Kluwer Academic/Plenum Publishers, New York.

Turowski, J. M., N. Hovius, H. Meng-Long, D. Lague, and C. Men-Chiang (2008), Distribution of erosion across bedrock channels, *Earth Surf. Processes Landforms*, *33*(3), 353–363, doi:10.1002/esp.1559.

Wegmann, K. W., and F. J. Pazzaglia (2002), Holocene strath terraces, climate change, and active tectonics: The Clearwater River basin, Olympic Peninsula, Washington State, *Geol. Soc. Am. Bull.*, *114*(6), 731–744, doi:10.1130/0016-7606(2002)114<0731:HSTCCA>2.0.CO;2.

Wellmeyer, J. L., M. C. Slattery, and J. D. Phillips (2005), Quantifying downstream impacts of impoundment on flow regime and channel planform, lower Trinity River, Texas, *Geomorphology*, *69*(1), 1–13.

Whipple, K. X., and G. E. Tucker (1999), Dynamics of the stream-power river incision model: Implications for height limits of mountain ranges, landscape response timescales, and research needs, *J. Geophys. Res.*, *104*(B8), 17,661–17,647, doi:10.1029/1999JB900120.

Williams, G. P. (1986), River meanders and channel size, *J. Hydrol.*, *88*(1–2), 147–164, doi:10.1016/0022-1694(86)90202-7.

Wobus, C. W., B. T. Crosby, and K. X. Whipple (2006a), Hanging valleys in fluvial systems: Controls on occurrence and implications for landscape evolution, *J. Geophys. Res.*, *111*, F02017, doi:10.1029/2005JF000406.

Wobus, C. W., G. E. Tucker, and R. S. Anderson (2006b), Self-formed bedrock channels, *Geophys. Res. Lett.*, *33*, L18408, doi:10.1029/2006GL027182.

Wohl, E., P. L. Angermeier, B. Bledsoe, G. M. Kondolf, L. MacDonnell, D. M. Merritt, M. A. Palmer, N. L. Poff, and D. Tarboton (2005), River restoration, *Water Resour. Res.*, *41*, W10301, doi:10.1029/2005WR003985.

Wolkowinsky, A. J., and D. E. Granger (2004), Early Pleistocene incision of the San Juan River, Utah, dated with 26Al and 10Be, *Geology*, *32*(9), 749–752, doi:10.1130/G20541.1.

Yanites, B. J., and G. E. Tucker (2010), Controls and limits on bedrock channel geometry, *J. Geophys. Res.*, *115*, F04019, doi:10.1029/2009JF001601.

Yanites, B. J., G. E. Tucker, K. J. Mueller, and Y.-G. Chen (2010), How rivers react to large earthquakes: Evidence from central Taiwan, *Geology*, *38*(7), 639–642, doi:10.1130/G30883.1.